Modeling of Current–Voltage Characteristics of Thin-film Solar Cells Incorporating Bulk and Surface Recombination: application to perovskite solar cells

Sheikh Mohammad Shuvoraj

A Thesis

in

The Department

of

Electrical and Computer Engineering

Presented in Partial Fulfillment of the Requirements

for the Degree of Master of Applied Science (M.A.Sc) at

Concordia University

Montreal, Quebec, Canada

November 2023

CONCORDIA UNIVERSITY

School of Graduate Studies

This is to certify that the thesis prepared

By: Sheikh Mohammad Shuvoraj

Entitled: Modeling of Current–Voltage Characteristics of Thin-film Solar Cells Incorporating Bulk and Surface Recombination: application to perovskite solar cells

and submitted in partial fulfillment of the requirements for the degree of

Master of Applied Science

complies with the regulations of this University and meets the accepted standards with respect to originality and quality.

Signed by the final Examining committee:

_____ Chair
Dr. Steve Shih

_____ Examiner, External
Dr. Muthukumaran Packirisamy To the Program

_____ Examiner
Dr. Steve Shih

_____ Supervisor
Dr. M. Z. Kabir

Approved by: _____
Dr. Yousef R. Shayan, Chair
Department of Electrical and Computer Engineering

_____20_____ _____
Dr. Mourad Debbabi, Dean
Faculty of Engineering and Computer Science

ABSTRACT

Modeling of Current–Voltage Characteristics of Thin-film Solar Cells Incorporating Bulk and Surface Recombination: application to perovskite solar cells

Sheikh Mohammad Shuvoraj

Photovoltaic solar cell is one of the most important renewable energy sources, which can supply required energy to various electronic devices as well as enormous energy to power grids. Among various photovoltaic devices, thin-film solar cells provide high power conversion efficiency at lower production cost. Though they provide reasonably high efficiency, there is possibility to improve the efficiency further through properly understanding the efficiency limiting factors. To achieve this goal, a physics-based compact analytical model for studying the carrier distribution and resultant photocurrent alongside with the current-voltage (J-V) characteristics of bulk heterojunction (BHJ) perovskite solar cells (PSC) has been proposed in this thesis by considering exponential photon absorption profile, bulk and surface recombination, and carrier drift & diffusion in the photon absorption layer.

By solving the continuity equation for both electrons and holes in the perovskite layer, it is possible to construct an analytical formula for the position-dependent carrier concentration and associated external voltage-dependent photocurrent. The position dependent total conduction current (sum of the drift and diffusion currents of both holes and electrons) under steady-state is found to be space invariant which is exactly equal to the total photocurrent calculated using the Shockley-Ramo's theorem. The calculation of the total load current considers the actual solar spectrum, photocurrent and voltage-dependent forward dark current. The mathematical model is fitted with experimental results of various perovskite solar cells and useful physical transport parameters are extracted by comparing the model calculations with the published experimental data. The effects of recombination on the photocurrent and overall efficiency are analysed quantitatively. The charge carrier transport parameters, especially the surface recombination velocity, have very significant effects on the current-voltage characteristics and power conversion efficiency.

ACKNOWLEDGMENT

All praises belong to Almighty who gave me the health, strength, and ability to complete my thesis.

I would like to express my deepest gratitude and appreciation to my thesis supervisor Dr. Zahangir Kabir for his guidance, encouragement, and financial support throughout the progress of the work. This thesis would not have been completed without his support and guidance. I would like to express my great thanks and gratefulness for his instructions, continuous encouragement, valuable discussions, and careful review during the period of this research. His keen sight and a wealth of farsighted advice and supervision have always provided me the precise guiding frameworks of this research. I have learned many valuable lessons and concepts which I have utilized to develop my abilities to work innovatively and to boost my knowledge.

Finally, I would like to give special thanks to my friends and family for their great assistance. And a very special thanks to my beloved wife, Rezowana Roich, who has always been my key emotional support.

TABLE OF CONTENTS

LIST OF FIGURES

LIST OF TABLES

LIST OF SYMBOLS

q - Elementary charge

h - Planck's constant

c - Velocity of light

λ - Wavelength of the incident photon

V_{oc} - Open circuit voltage

J_{sc} - Short circuit current density

R_s - Series area resistance

R_p - Parallel area resistance

μ_n - Mobility of electron

μ_p - Mobility of hole

τ_n - Electron lifetime

τ_p - Hole lifetime

k - Boltzmann's constant

T - Absolute temperature

D_n - Diffusion coefficient of electron

D_p - Diffusion coefficient of hole

ϕ_n - Electron injection barrier

ϕ_p - Hole injection barrier

V_{bi} - Built-in potential

α - Absorption coefficient of the material

L_n - Diffusion length of electron

L_p - Diffusion length of hole

V_t - Thermal velocity

W - Active layer width

δ_n - Excess photo-generated electron concentration

δ_p- Excess photo-generated hole concentration

G- Carrier Generation Rate

I_o- Intensity of the solar radiation

LIST OF ABBREVIATION

AM - Air mass

BHJ - Bulk heterojunction

EHP - Electron and hole pair

HOMO - Highest occupied molecular orbital

ITO - Indium tin oxide

PCBM= [6,6]-phenyl C61-butyric acid methyl ester

LUMO - Lowest unoccupied molecular orbital

PSC - Perovskite solar cell

PCE - Power conversion efficiency

SRH - Shockley-Read-Hall

$MAPbI_{3=}$ Methylammonium lead triiodide

$FAPbI_3$=Formamidinium lead iodide

ETL= Electron Transport Layer

HTL= Hole Transport Layer

CHAPTER 1: INTRODUCTION

1.1 Brief literature review and motivation

The development of renewable energy is now more important than ever because of the threats posed by global warming and climate change, as well as the understanding of the significance of achieving carbon neutrality. The most popular option for future energy sources is the use of solar cells that capture pure, inexhaustible, and easily accessible solar energy. Solar energy is a very promising, plentiful, environmentally friendly, and sustainable resource with the potential to drastically cut or possibly completely replace traditional energy sources. To do this, various ground-breaking photovoltaic technologies have been developed, but there is still a demand for solar cells that are affordable and have a high-power conversion efficiency.

Hybrid compounds (CH_3NH_3-PbX_3, X = I, Br, Cl) with organic and inorganic components and having unique perovskite crystal structure, are one of the most advanced technologies in the area. Perovskite solar cells (PSCs) use perovskite materials as light-absorbing substances. Their remarkable optoelectrical qualities have attracted a lot of interest for using those in making solar cells. Kojima et al. were the first to use $MAPbI_3$ perovskite solar cell reaching a power conversion efficiency (PCE) of 3.8% [1]. Surprisingly, perovskite solar cells (PSCs) swiftly outperformed this benchmark by now and attained a certified record PCE of 25.5%, presenting them as formidable candidates for the upcoming PV technology generation [2].

PSCs are superior to traditional solar cells in several ways. Simple manufacturing, a variety of device topologies , small and tunable energy band gaps, excellent carrier mobility , the capacity to absorb sunlight across a wide range of wavelengths, superior carrier diffusion length, higher carrier lifetimes and many other unique qualities have made them prominent in harvesting solar energy. The common formula ABX_3 can be used to indicate the typical arrangement of organic-inorganic lead halide perovskites. In this composition, A stands for a positive ion, Lead (Pb) is represented by B, and halogens are represented by X . Modern perovskite solar cells (PSCs) can be divided into two different device configurations at this time: the regular (n-i-p) structure and the inverted (p-i-n) structure. The electron transport layer (ETL) is denoted by n, perovskite layer by i and hole transport layer (HTL) by p, respectively. In the conventional arrangement, the perovskite active layer is positioned between ETL and HTL.

The optoelectronic characteristics of various interfaces, such as the electrode/ETL, ETL/perovskite, perovskite/HTL, and HTL/electrode interfaces, are extremely important in determining the stability as well as the performance of the device . Therefore, to develop PSCs with the maximum potential power conversion efficiency (PCE), it is thought to be necessary to have a fundamental grasp of the optoelectronic properties of perovskite materials. To achieve maximum values for metrics like short-circuit current (I_{sc}), open-circuit voltage (V_{oc}), and fill factor (FF), however, both the materials used, and the interfaces present within the device are equally important.

The main goal of earlier investigations was to enhance the performance of PSCs by addressing perovskite film technology and applying passivation techniques to reduce flaws in the bulk

material or at grain boundaries. These procedures involved composition changing, additive engineering, and processing techniques. For example, by switching the material composition from $MAPbI_3$ to $FAPbI_3$ since 2015, researchers have produced relatively high-power conversion efficiencies (PCEs) [3]. To stabilise the phase of $FAPbI_3$ at room temperature, little portion of MA cation and Br anion were added to the compound.

The significance of interface engineering has been underlined in more recent papers for further improved the effectiveness and stability of PSCs. In perovskite solar cells, the presence of interfaces has a significant impact on the extraction and injection of carriers. Deep level traps may be present at these interfaces and cause considerable charge accumulation and recombination, lowering the open-circuit voltage (V_{oc}), fill factor (FF), and overall device performance. As a successful modification method, interface engineering lessens nonradiative recombination at the layer surface, prevents the unintended movement of heterogeneous carriers, and strengthens the bond between the top and bottom layers.

Modeling the current-voltage properties of perovskite solar cells has only been the subject of a few research publications. By quantitatively resolving Poisson's and continuity equations, Sherker et al. [4] proposed the drift-diffusion model. However, the fundamental characteristics of dark current were not considered in the model they created. Sun et al. [5] created an analytical model for perovskite solar cells in a separate work. However, this model disregarded the major impact of bulk carrier recombination on both the dark and photocurrents. Under the influence of the underlying electric field, the photogenerated electrons and holes move through the perovskite layer, but some of these carriers are lost due to bulk recombination.

The key parameters affecting the efficiency of power conversion are photon absorption, recombination procedures like Shockley-Read-Hall (SRH) recombination and surface recombination, as well as the dark current. Shockley-Read-Hall (SRH) recombination with non-radiative trap assistance is the main recombination process in perovskite solar cells [6]. Additionally, a key factor in lowering the carrier concentration at the surfaces is the surface recombination velocity. Reduced charge collection efficiency for the photogenerated carriers results from a decrease in the effective built-in electric field at the operational voltage due to both bulk and surface recombination. Therefore, it is vital to develop a physics-based compact model considering charge carrier transport including both bulk and surface recombination.

1.2 Research objectives

This thesis investigates how the current-voltage characteristics of solar cells are affected by the charge carrier properties of bulk and interface layers. With the aim of enhancing overall efficiency and device performance, the objective is to provide a thorough understanding of how the variations in perovskite material composition and interface engineering can affect charge carrier transport, including mobility, lifetime, and surface recombination. A physics-based analytical model is developed to forecast prospective carrier transport characteristics that could maximise the power conversion efficiency. The research endeavour is organised into numerous tasks to achieve these goals.

- The first objective entails the development of a physics-based model that accurately predicts the photocurrent in perovskite solar cells while taking into consideration the contact effect and appropriate boundary conditions. By integrating the carrier recombination and dark-current effect, the model seeks to determine the net external current of the cell.

- The second task includes the application of the analytical model created in the preceding task with results of published experimental data. With varying material compositions and interface layers, the goal of this comparison is to examine how charge carrier transport of the bulk material and interface properties affect the efficiency of perovskite solar cells. In addition, the charge transport and interface properties of the cell are extracted by fitting the model with the experimental data.

1.3 Organization of the thesis

The thesis is structured as follows:

Chapter 2 covers essential background information required to grasp the research in this thesis. This includes an examination of the composition and characteristics of perovskite solar cells, as well as their operational principles. Additionally, it briefly discusses the up-to-date research on various methodologies of increasing the PCE performance of PSC with composition and interface engineering.

In Chapter 3, we introduce voltage-dependent photo current models to show the effect of surface recombination and bulk recombination. Apart from the conventional Shockley-Ramo's theorem, a different approach to calculate the total current from the carrier concentration was developed to understand the effect of different transport parameter on position dependent carrier concentration and photocurrent.

Chapter 4 presents a voltage-dependent photocurrent model revealing the effect of bulk and surface recombination on the total photocurrent and overall efficiency. Consideration is given to series and parallel resistances in order to obtain the net external photocurrent. Furthermore, we validate the model by fitting it to experimental data and showcase the impact of parameters like series resistance, carrier mobility, surface recombination velocity, and carrier lifetime on the current-voltage characteristics.

Lastly, Chapter 5 provides a conclusion to the thesis, summarizing its significant findings and highlighting potential avenues for future research and improvement.

CHAPTER 2: BACKGROUND THEORY

2.1 Introduction

The purpose of this chapter is to provide necessary background knowledge regarding perovskite solar cells (PSC). It includes the perovskite structure, device architecture, working principle, significant terms related to current-voltage (J-V) characteristics of a perovskite solar cell.

2.2 Perovskite Crystal Structure

Perovskites are chemical compounds that follows the formula ABX_3 where X is a negatively charged ion, A is mainly organic cation and B is metal cation (A is larger than B). The crystal structure of perovskites is shown in **Figure 2.1**. The tolerance factor, indicated as t, and the octahedral factor, denoted as μ mainly define the expected structure of perovskites and their crystallographic stability. The ratio of the distances between A-X to B-X in an idealised solid-sphere model is known as the tolerance factor *t* where,

$$t = \frac{R_A + R_X}{\sqrt{2}(R_B + R_X)}$$

Here, R_A, R_B, and R_X stand for the ionic radius of the respective ion. The ratio of R_B to R_X is defined by the octahedral factor, μ. The typical range of values for t and μ for halide perovskites (X = F, Cl, Br, I) is 0.81 to 1.11 and 0.44 to 0.90, respectively [7]. For better performance, perovskites should have a cubic structure similar to the one shown in **Figure 2.1.** It is possible if value of t, lies within the range of 0.89 to 1.0. For the lower values of t, the structures can be less symmetrical like tetragonal or orthorhombic structures.

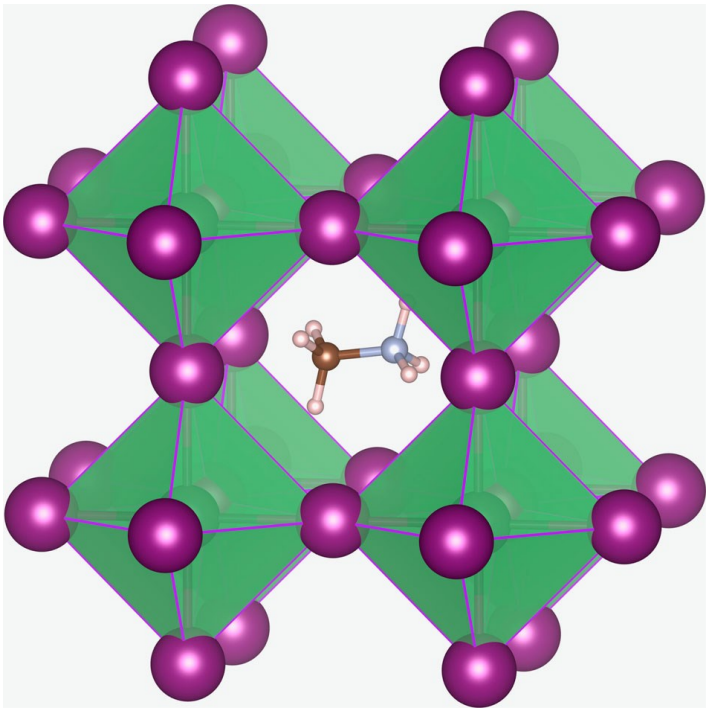

Figure 2.1: The crystal structure of perovskites material. MA cation (CH3NH3+) occupies the central A site surrounded by iodide ions in corner-sharing PbI_6 octahedra. (ref 8)

The bigger cation A is typically methylammonium ($CH_3NH_3^+$) with an ionic radius of R_A = 0.18 nm. Besides, formamidinium ($CH(NH_2)_{2+}$) is also widely used now a days. The cation B has always been Pb (R_B = 0.119 nm) in high-efficiency solar cells. Besides, Sn (R_B = 0.110 nm) also shows a great promise as an alternative of Pb. Although Sn has more perfect bandgap theroritically, it typically has lesser stability. Generally, X is a halogen, most commonly iodine (R_X = 0.220 nm). However, Bromine and Chlorine are also widely used (R_X = 0.196 nm and 0.181 nm, respectively) in mixed halide compositions. Therefore, the mostly used chemical composition in this context is methylammonium lead triiodide ($CH_3NH_3PbI_3$). However, mixed halides like $CH_3NH_3PbI_{3-x}Cl_x$ and $CH_3NH_3PbI_{3-x}Br_x$ are also quite important.

2.3 Device Architecture

Five essential layers make up the multilayered architecture of perovskite solar cells (PSCs): a metal electrode, an electrode made of transparent material, a layer of electron transport (ETL), an active layer of perovskite material, and a hole transport layer (HTL). Each layer performs a specific task that aids in the photovoltaic process.

The active layer is responsible for absorbing sunlight and producing free charges. The ETL (or HTL) pulls electrons (or holes) out of the perovskite layer and moves them to the cathode (or anode) to minimise the recombination loss of charges. These intermediary layers also require careful design to correct for any energy imbalance between the energy levels of the perovskite layer and the electrodes. **Figure 2.2** illustrates the basic structures of common perovskite solar cells.

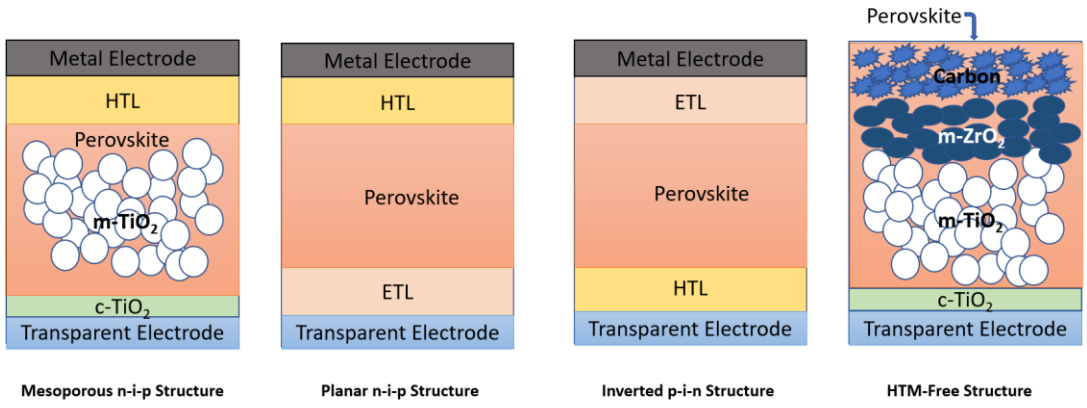

Figure 2.2: Commonly used device structures of PSC (adapted from Fig.4 of ref 9)

The internal structure of a perovskite solar cell (PSC) is a crucial factor for overall device performance. Depending on the arrangement of the radiation receiving layer exposed to incident light, PSCs can be divided into two categories: Inverted (p-i-n) and regular (n-i-p) structures.

2.4 Operation Principle of Perovskite Solar Cell

The operational principle of perovskite solar cells is similar to thin-film solar cells. The basic workings of PSCs are illustrated schematically in **Figure 2.3.** Perovskite layer acts as light-absorbing component for photovoltaic conversion and the other layers contribute to the efficient charge collection. Four crucial processes make up the photovoltaic process in PSCs: 1. light energy harvesting, 2. free electron and hole creation, 3. drift and diffusion of charges, and 4. charge collection at the electrodes.

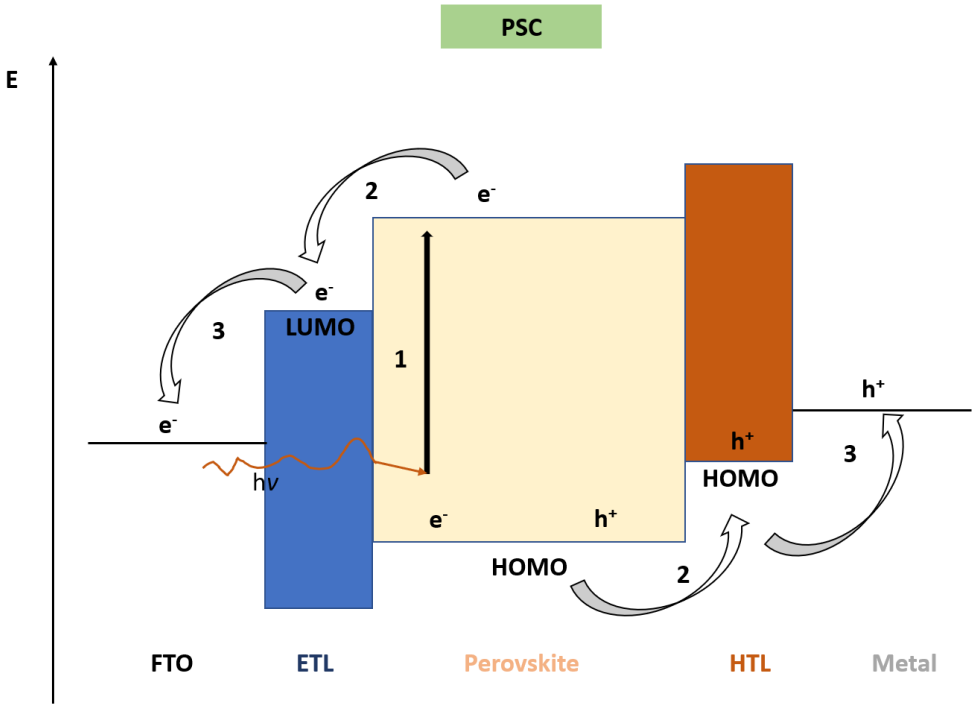

Figure 2.3: Working principle of PSC: 1. Photon absorption and free charges generation; 2. Transportation of charges; 3. Extraction of charge (adapted from Fig.6 of ref 10)

Perovskite solar cells (PSCs) produce electron-hole pairs by absorbing solar energy when sunlight shines on them. Electrons move towards the anode, made of glass fluorinated with tin oxide (FTO), after leaving the electron transporting layer (ETL). The holes are trangferred simultaneously through the hole transporting layer (HTL) until it reaches the metal cathode. While the counter electrode gathers holes, the working electrode is responsible for collecting electrons. The external circuit is then used to carry these charges, producing current as a result.

2.5 Carrier Transport and Collection Parameters

To get the optimal power from a solar cell, the photogenerated electrons and holes (carriers) must be separated, transported, and collected efficiently. Therefore, the overall performance of photovoltaic devices is greatly influenced by carrier transport and recombination. Recombination lifetime (τ), diffusion length (L_D), and recombination coefficients (k_n) are the main transport parameters of the charges that directly affect the efficiency of a PSC. These parameters can be fine tuned by changing the perovskite material composition. For instance, the mixed perovskite of $FAPbI_3$ with $MAPbI_3$, displays significantly higher L_D and carrier concentrations than pure $MAPbI_3$. This shows that the mixed perovskite based on $FAPbI_3$ may have better photovoltaic performance than $MAPbI_3$[11].

2.6 I-V Characteristics of Solar Cell

The commonly used circuit configuration for solar cell is depicted in **Figure 2.4.** A current source, a single diode, and two resistors—one in series and one in parallel are shown as the most typical circuit representation for a solar cell. An ideal solar cell should behave like a current source. But

for considering different kind of losses and dark situation, the ideal model is linked with diode including some additional resistor in the circuit to describe the operation more accurately [12].

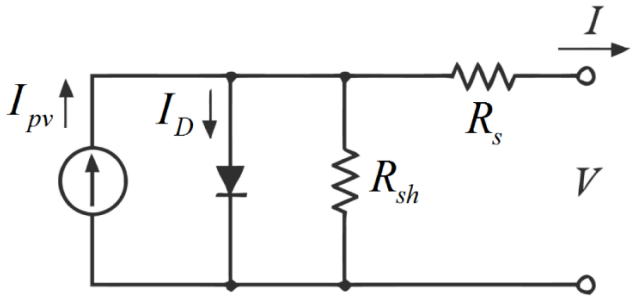

Figure 2.4: Equivalent circuit of a solar cell (ref 13 Fig 1)

The following equation can be used to explain the current-voltage (I-V) curve of an PSC:

$$I(V) = I_d(V) - I_{ph}(V) + \frac{V - IR_s}{R_{sh}} \qquad \textbf{2.1}$$

Here, the applied bias is V and corresponding net external current is I (V). I_{ph}(V) stands for the photocurrent generated by the solar irradiation, I_d (V) is responsible for dark current developed from the bias in the dark situation. R_s is the series resistor accounted for losses in solder bonding, interconnections, junction boxes, etc whereas R_{sh} stands for the shunt resistor that accounts for current leakage through high conductivity shunts across the p-n or p-i-n junctions.

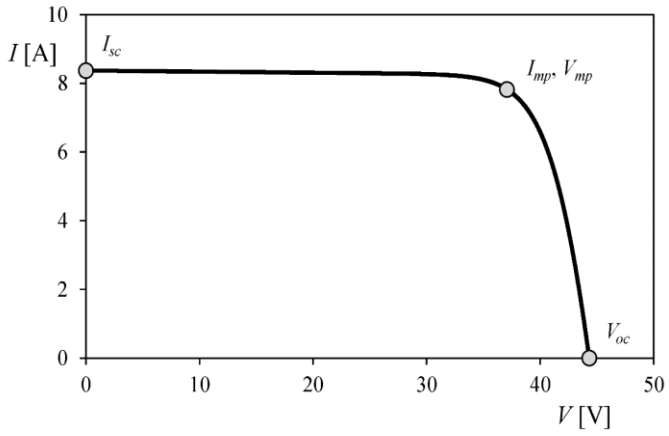

Figure 2.5: I-V curve of a solar panel. The three characteristic points (short circuit, maximum power, and open circuit points) are indicated on the curve (ref 13 Fig 2)

The open circuit voltage (V_{oc}), short circuit current (I_{sc}), fill factor (FF), power conversion efficiency (PCE), series resistance (R_s), and parallel resistance (R_{sh}) are the characteristics included in the I-V curve that are used to evaluate the performance of a solar cell.

2.6.1 Short Circuit Current (Isc)

When the externally supplied voltage is zero, a short circuit condition at the output terminal is indicated by a current known as the short circuit current (I_{sc}). Under this short-circuit scenario, I_{sc} stands for the net current in the external circuit. **Figure 6** shows how I_{sc} appears on the I-V curve. In an ideal condition, the photocurrent and the short-circuit current are expected to be equal.

2.6.2 Open Circuit Voltage (Voc)

The maximum voltage a solar cell may produce when its terminals are left open is known as the open circuit voltage. V_{oc} mostly depends on the work function of the metal contacts. Theoretically, this is modeled by the situation when the photocurrent and dark current totally cancel each other.

The open circuit voltage V_{oc} is increased logarithmically with light intensity and can be described by the following equation [12]:

$$V_{oc} = \frac{kT}{q} \ln \left(\frac{I_{sc}}{I_o} + 1\right)$$

where k= Boltzmann constant, T= Temperature (K), I_o = reverse saturation diode current.

The expression for the V_{oc} may not be valid for all types of solar cell structure and can be found only when the short circuit current (I_{sc}) is exactly equal to the diode like dark current and cancel each other where the dark current is characterised by the following expression:

$$I_{dark} = I_o \exp \left(\frac{qV}{kT} - 1\right)$$

2.6.3 Fill Factor (FF):

The performance of a solar cell is characterized by the fill factor (FF), which can be calculated from the I-V curve using the formula below:

$$FF = \frac{I_{mp} V_{mp}}{I_{sc} V_{oc}}$$

The maximum output power is represented by I_{mp} and V_{mp} in this case, which stand for the current and voltage at the maximum power point, respectively. According to the equation, FF stands for the ratio of the maximum output power to the maximum achievable output power that can be gained from the solar cell. In terms of graphics, it depicts the "squareness" of the solar cell and establishes the size of the biggest rectangle that can be contained by the I-V curve.

2.6.4 Power conversion efficiency (PCE):

The efficiency η of a solar cell is the ratio of maximum output to input power and is determined using the formula:

$$\eta = \frac{P_m}{P_{in}} = \frac{V_{oc} I_{sc} FF}{P_{in}}$$

where P_{in} is the input optical power from the incident light. The four parameters: I_{sc}, V_{oc}, FF and η are the main performance indicator of a solar cell and dependent on illumination condition. So, proper illumination condition should be defined for accurate determination of these parameters.

2.6.5 Series resistance (Rs)

Series resistance (Rs) is the sum of the contact resistance between the semiconductor and electrodes; and the internal resistance of the electrode materials raised from the movement of charge carriers inside the semiconductor materials. High series resistance can lower I_{sc} significantly which can affect the fill factor.

2.6.6 Shunt or parallel resistance

Shunt or parallel resistance R_{sh} can cause a solar cell to lose a large amount of power. Light-generated carriers may proceed along different pathways as a result of manufacturing flaws,

eventually resulting in recombination. Low parallel resistance can cause these carriers to take these alternate routes, which reduces the photocurrent flow through the external circuit.

2.7 Charge Recombination Effect in Solar Cell

Recombination procedures can be divided into several categories. The majority of the literature makes a distinction between bulk and surface recombination. It can also be classified as radiative and non radiative recombination [14]. Various processes of recombination are illustrated in **Figure 2.6.**

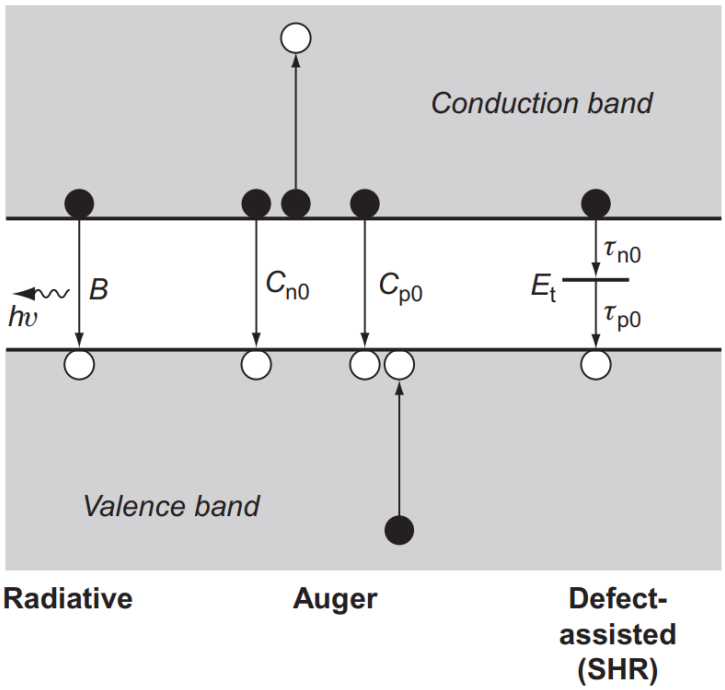

Figure 2.6: Different Types of recombination (ref 14 Fig 9)

Radiative recombination is mainly band-to-band recombination. In this process, the electron directly switches from a state in the conduction band to an unoccupied state in the valence band. The electron releases its stored energy during recombination process in form of photons or radiation. That is why the process is called radiative recombination.

Radiation less or nonradiative recombination is the process where there is no photon emission. In a non radiative recombination, trap levels within the bandgap facilitate the recombination process. The recombination process that incorporates a mid gap state, frequently uses a multi phonon mechanism. Instead of emitting photons in this operation, the energy is released as lattice vibrations (phonons). Nonradiative recombination can be linked to defects that are present in bulk or surface of the semiconductor material.

In semiconductor devices, recombination through midgap states has a big impact. Nonradiative recombination is less likely to occur in the materials that have wider band gap [15]. As a result, non-radiative recombination is more probable in the presence of a midgap state, which may effectively trap both electrons and holes. This kind of recombination is typically described by the Shockley-Read-Hall (SRH) recombination model. An electron from the conduction band and a hole from the valence band are both caught in a localised state within the bandgap in this recombination process.

There can be multiple defect sites at the semiconductor interfaces. Surfaces (including interfaces) introduce electronic state bands within the band gap, much like dislocations and planar defects like grain boundaries. Surface recombination is the term used to describe recombination that occurs at these surface spots. Recombination at the surfaces is characterized by the surface recombination velocity.

Understanding surface recombination is pivotal as it is an important factor that affects the dark saturation current and the quantum efficiency of solar cells. Surface roughness, pollution, and the

presence of ambient gases during oxidation and annealing are only a few of the variables that have a significant impact on the surface recombination velocity. Surface recombination can be reduced by using a passivating layer to ensure maximum performance.

Auger recombination is another important phenomenon in strongly doped inorganic semiconductors. It entails the transfer of energy from one electron or hole to another electron or hole that is released during the band-to-band recombination of an electron and a hole (as shown in **Figure 2.6**). As a result, the third particle, which is usually an electron, gets kinetic energy. However, once the carrier relaxes back to the energy at the band edge, this extra energy usually dissipates.

The rate equation $dn/dt = -k_1n - k_2n^2 - k_3n^3$ can be used to describe the recombination of charge carriers in semiconductors where n is the electron charge-carrier density. The first-order Shockley-Read-Hall (SRH) trapping rate constant (also known as monomolecular recombination) is denoted by k_1 whereas k_2 is the second-order band-to-band (radiative) recombination rate constant (referred to as "bimolecular recombination" due to the reaction of electron and hole), and k_3 defines the third-order auger recombination rate constant [16].

2.8 Compositional Engineering

Compositional engineering is frequently used to modify the chemical configurations between the perovskite components to improve the performance of perovskite solar cells. This modification can change the power conversion efficiency (PCE) of the devices as well as their thermodynamic and environmental stability, in addition to the optoelectronic properties of the materials. In this

section, a closer look will be taken at the important roles that each component performed in this technique and developed a summary of successful tactics achieved so far.

2.8.1 A cation-Modification

A cation has relatively little effect on the optoelectronic properties of perovskite materials compared to the B- and X-site ions. Generally, A cation acts as a geometric spacer for the corner-sharing PbI_6 octahedra, preventing distortion. As a result, the bond length and angle between Pb^{2+} and the halide ions can depend on the size and symmetry of the A cation. This affects the distribution of the band edge states. [17]. It is found that $APbI_3$ perovskite bandgap may vary from about 1.5 to 1.7 eV and the varition can be dependent on A cation size.

2.8.1.1. $MAPbI_3$

For a long period, the methylammonium (MA) cation-based perovskite material was carefully examined for its potential in solar applications. For polycrystalline films, the charge-carrier mobility ranged from 1 to 70 $cm^2/(V\text{-}s)$ and the bandgap of single-crystal $MAPbI_3$ was determined to be 1.51 eV [18]. But in terms of stability, dynamic reorientation of the organic MA cations inside the octahedral cage has been seen to occur within a very short period. The application of $MAPbI_3$ is constrained by few unfavourable characteristics, such as its low reversible phase transition temperature, sensitivity to deterioration in the presence of moisture, and poor thermal stability.

2.8.1.2. $FAPbI_3$

In comparison to $MAPbI_3$, formamidinium lead triiodide ($CH(NH_2)_2PbI_3$ or $FAPbI_3$) demonstrates better temperature stability. Furthermore, the bandgap of $FAPbI_3$ is 1.48 eV, which is closer to the "ideal" bandgap range of roughly 1.1-1.4 eV for single-junction solar cells and allows for effective absorption of solar photons [19].

While their electrical band structures and absorption coefficients are comparable, the cubic $FAPbI_3$ phase exhibits a considerably narrower bandgap than the thin film of $MAPbI_3$ despite distortion. Additionally, it was discovered that $FAPbI_3$ films had much longer charge-carrier lifetimes and diffusion lengths than $MAPbI_3$ films. A relatively small number of devices based only on pure $FAPbI_3$ films have achieved PCE surpassing 19%, however, because to the poor phase stability of $FAPbI_3$.

2.8.1.3. Mixed A-Cation

In comparison to pure perovskite materials, perovskite compounds that include organic cations of formamidinium (FA) and methylammonium (MA) have shown increased performance and stability. Even though FA provides many benefits, MA keeps the perovskite structure stable and prevents it from changing into the yellow polymorph (which possesses a structure resembling a chain to impede the flow of electrons and diminish photovoltaic efficiency), commonly known to happen with FA-based perovskites [20]. The increased size of the FA cation makes it difficult to fit it into the cuboctahedra site which is the main cause of environmental instability of $FAPbI_3$. Mixing up FA cation with smaller MA cation may help in keeping the cubic perovskite phase at room temperature.

Wu et al. achieved a remarkable power conversion efficiency (PCE) of 18.21% [21] in an inverted perovskite solar cell (PSC) with a mixed cation/halide perovskite composition of

$FA_{0.85}MA_{0.15}Pb(I_{0.85}Br_{0.15})_3$. The use of a perovskite-fullerene graded heterojunction (GHJ) structure considerably improves the photovoltaic performance of the PSCs with high PCE.

However, the advantageous photo and thermal stabilities demonstrated by $FAPbI_3$ perovskite films were degraded as a result of the partial replacement of FA by MA in perovskite films. Yellow phase impurities, even in trace levels, have a major impact on film shape and crystal development, which hinders charge collection and reduces device performance. Even for high-efficiency PSCs, it is difficult to produce perovskite films without detectable amounts of the yellow phase, despite the mixed FA/MA perovskites shows good performance. In contrast to the $FAPbI_3$ film, the $FA_{0.5}MA_{0.5}PbI_3$ film degrades more quickly and entirely after about 8 hours of illumination [22]. Instead of MA, this problem has been solved by using the cesium (Cs) cation. Solar cells were more stable and reproducible as Cs cation has better stability under moisture and light [23]. The addition of Cs cations to the FA/MA mixed-cation perovskite leads to increased crystallinity, decreased defect density and boosted photovoltaic performance.

Tan et al. used the mixed cation-halide perovskite $Cs_{0.05}FA_{0.81}MA_{0.14}PbI_{2.55}Br_{0.45}$ using an antisolvent technique to create planar perovskite solar cells with an active area of 1.1 cm^2 and a certified PCE of 19.5% [24] was achieved.

In order to further improve the functionality and stability of perovskite films and devices, complex multi-cation systems have also been investigated as a result of the creation of alternative cations. Lu et al. recently developed efficient and stable perovskite solar cells [25] by altering the perovskite interface. One-step antisolvent fabrication of the perovskite solar cells with a remarkable PCE of 19.6% was made possible while maintaining great stability.

2.8.2 B cation-Modification

Given the toxicity issues with Lead, a lot of research has gone into developing alternatives to Pb-based perovskite materials for high-efficiency solar cells. Sn-based perovskites have the potential to partially replace their Pb-based counterparts among the alternative choices. With four valence electrons in its s and p orbitals, Sn has a similar valence electron configuration to Pb, which enables Sn-based perovskites to have comparable optoelectronic properties. Sn^{2+} has a different band structure and favorable bandgap than Pb^{2+} due to its smaller ionic radius. The bandgaps of Sn-based iodide perovskites, such as $CsSnI_3$, $MASnI_3$, and $FASnI_3$, have been measured to be in the range of 1.3–1.4 eV [26], making them more appropriate for single-junction solar cells than Pb-based iodide perovskites because of their higher bandgaps.

Researchers have looked towards partially replacing Pb with Sn in perovskite materials to overcome the drawbacks of pure Sn-based perovskites. Compared to pure Sn-based perovskites, these mixed Sn-Pb perovskites show better stability. Lin et al. used a device based on perovskite $MA_{0.3}FA_{0.7}Pb_{0.5}Sn_{0.5}I_3$ to achieve a high PCE of 21.1% by adding metallic Sn to the precursor solution [27]. With appropriate crystal growth and defect engineering, mixed Sn-Pb perovskites have the potentiality to surpass pure Pb-based perovskite solar cells for better PCE.

2.8.3 X anion-Modification

The optoelectronic properties of metal halide perovskites can be changed by substituting iodine (I) with other halide anions like chlorine (Cl-) and bromine (Br-). The substitution of the X-site anion has a substantial impact since it directly affects the band edge states of the perovskite materials.

The selection of the halide anion has a significant impact on the photoelectric characteristics, film morphology, and photovoltaic performance of $MAPbX_3$ perovskites.

Cl-, Br-, and I- are the three mostly often utilised halide anions. Iodide-based perovskite materials are preferable for solar applications because of their smaller bandgap, which enables larger light absorption. However, due to characteristics like its greater departure from the ideal tolerance factor, lower I- electronegativity, and weaker binding with the Pb^{2+} ion, $MAPbI_3$ is the least stable material of the three [28]. Partial substitutions of I- with Br- or Cl- have been used to address these stability issues and fine-tune the characteristics.

2.8.3.1 Br/I Mixed Perovskites.

According to a study, adding bromine (Br-) ions to $MAPbI_{3-x}Br_x$ causes the creation of an ordered cubic phase, which is more stable for devices than the deformed tetragonal phase found in pure $MAPbI_3$. Due to the higher lowest unoccupied molecular orbital (LUMO) and lower highest occupied molecular orbital (HOMO) energy levels of $MAPbBr_3$ compared to $MAPbI_3$, solar cells based on $MAPbI_{3-x}Br_x$ also exhibit higher open-circuit voltages [29].

The average bond distance between lead (Pb) and halide (X) varies as a result of the replacement of the smaller bromine ion (Br-) in $MAPb(I_{1-x}Br_x)_3$, which in turn affects the bandgap of the perovskite thin films. According to the following equation: $E_g(x) = 1.57 + 0.39x + 0.33x^2$, the bandgap grows with increasing x [30], and the tolerance factor of $MAPb(I_{1-x}Br_x)_3$ similarly rises. As a result, when x is greater than 0.2, the crystal structure of $MAPb(I_{1-x}Br_x)_3$ transforms from tetragonal to cubic or pseudo-cubic. This transformation leads to improvements in the fill factor (FF) and open-circuit voltage (V_{oc}), even a little quantity of bromine incorporation greatly improves the photovoltaic conversion efficiencies (PCEs) of the solar cells.

However, because of the relatively high bandgap, bromine (Br) content in the perovskite structure over a certain amount will reduce the short-circuit current density and, as a result, the photovoltaic conversion efficiency (PCE) of the devices. The lower series resistance of the perovskite layer, which is probably connected to the enhanced crystallinity of the film, might be attributed to the higher fill factor (FF) found in devices with more bromine. Bromine insertion may encourage the long-range orderly development of perovskite crystals, resulting in improved charge-carrier transport capabilities, because it produces a more suitable tolerance factor.

2.8.3.2 Cl-Incorporated Perovskites

The addition of chloride (Cl-) to $MAPbI_3$ can improve the film shape without changing the absorption beginning at about 800 nm, according to theoretical estimates [31]. Despite having comparable absorption characteristics, the electrical characteristics of perovskite differ significantly, indicating that Cl- is a key factor in influencing how charge carriers behave.

In comparison to $MAPbI_3$, $MAPbI_{3-x}Cl_x$ has faster carrier transport and longer carrier lifetimes. It is also more stable than $MAPbCl_3$ [32]. For instance, $MAPbI_{3-x}Cl_x$ films have electron and hole diffusion lengths that are roughly ten times longer than those of $MAPbI_3$ films. This demonstrates the crucial functions Cl- ions play in iodide-based perovskite films. There might be some effects of Cl- ions during crystallisation of the perovskite films. An intermediary phase of $MAPbI_{3-x}Cl_x$ is created which changes into $MAPbI_3$ eventually because of the volatilization of MACl from the film during $MAPbI_3$ perovskite production. The expansion of these intermediary phases encourages the creation of larger, more crystallin grains, which enhances the optoelectronic quality of the films.

2.9 Interface Modification

The perovskite layer, ETL/HTL for electron and hole transport, and transparent/metal electrodes are all essential layers that make up a typical perovskite solar cell (PSC). The electrode/ETL/ perovskite/HTL/electrode interfaces are the four primary interfaces between the layers. Since the characteristics of these interfaces have an immediate impact on procedures including charge extraction, transport, recombination, and photon transmission, they are essential for achieving high device performance.

Several noteworthy research have concentrated on improving solar cell performance through interface improvements. The reduction of non-radiative recombination losses is essential to reach the theoretical efficiency predicted by the Shockley-Queisser (SQ) theory [33], for improving the performance and long-term stability of perovskite solar cells (PSCs) . The efficiency of charge extraction and various photovoltaic parameters in PSCs are affected by interface-induced recombination and energy-level mismatch, in addition to losses inside the perovskite layer brought on by inherent defects. To alter the properties of interfaces and reduce interfacial losses without impairing the qualities of the bulk layers, interface engineering offers a practical and efficient method. Additionally, improving the interfaces can protect the entire device from deterioration, resulting in increased stability. The effect of interface engineering will be covered in more detail in the following section.

2.9.1 Defect Passivation

The performance of perovskite solar cells (PSCs) can be negatively impacted by the existence of deep-level defects at the surface and interfaces of perovskite materials. These defects can trap charge carriers and cause charge accumulation, recombination losses, and hysteresis. Particularly,

flaws at the top and bottom interfaces of the perovskite surface, which have higher recombination velocities than defects inside the bulk, significantly affect the charge carrier lifetimes.

Chemical interactions at the interfaces, such as electronic coupling and chemical binding, have been demonstrated to be useful interface engineering techniques for lowering trap states and minimising nonradiative recombination. By reducing the presence of deep-level defects, these methods can improve charge carrier dynamics overall and increase PSC performance.

To passivate interfacial flaws and produce high-performance perovskite solar cells (PSCs), numerous techniques have been used. For instance, the application of an ultrathin layer made of a combination of PMMA and PCBM close to the TiO_2/perovskite interface successfully passivated defects, leading to a noteworthy suppression of interfacial recombination and an improvement in V_{oc} with a rise of up to 80 mV [34]. Another method involves creating a bottom-up gradient at the ETL/perovskite interface using PCBM, which not only decreased defects within the grain boundaries but also passivated surface flaws [35]. Additionally, the addition of triphenylamino derivatives at the perovskite/HTL interface decreased the density of surface defects, enhanced band alignment, and raised V_{oc} [36]. These results show that the careful design of multifunctional molecules can result in defect passivation, providing a potential route to PSCs that are extremely effective and stable.

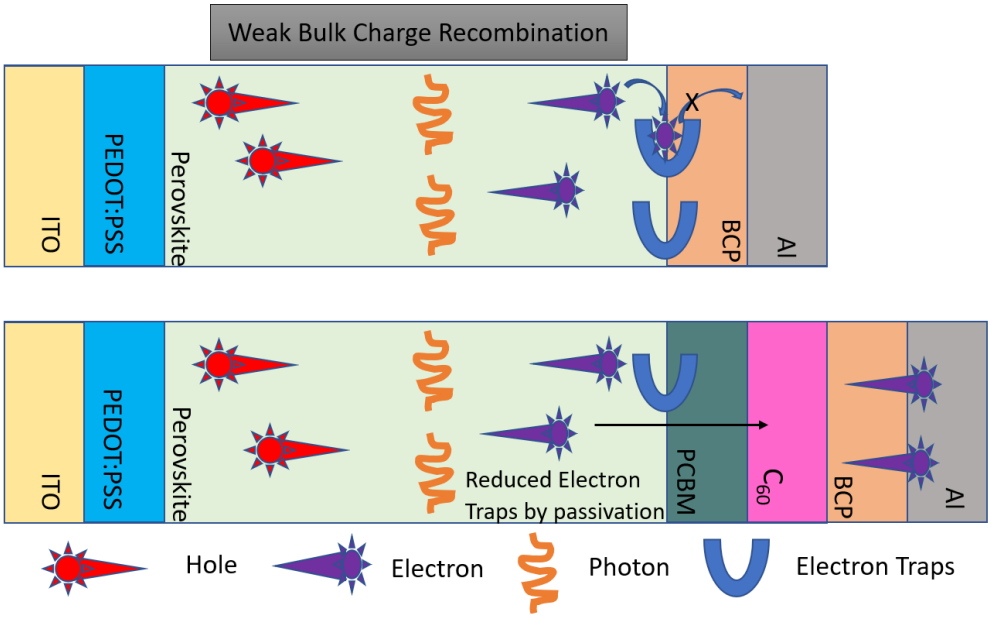

Figure 2.7: Schematic of the surface recombination reduction by passivating the trap states (adapted from Fig. 5c of ref 35)

2.9.2 Alignment of Energy Level

It is useful for boosting device performance to match the energy levels between the perovskite layer and the carrier transport layers (CTLs). The extraction and transport of carriers can be improved, and energy losses inside the devices can be reduced, by adjusting the energy level alignment between the perovskite layer and the contact layers, particularly the electron transport layer (ETL) and the hole transport layer (HTL).

It is widely known that the conduction band energy (E_c) of perovskite layer should be higher than the conduction band energy (E_c) of ETL while its valence band energy (E_v) should be lower than the valence band energy (E_v) of HTL. An effective way to adjust the energy levels is by interface engineering, which also minimises interfacial recombination and closes the energy gap. For instance, in one study, an interface modifier called adenine was used to modify the surface of a

NiO_x film. The energy offset between the perovskite layer and the HTL was decreased by 0.1 eV in the presence of a thin layer of adenine, which significantly raised the open-circuit voltage (V_{oc}). The device also showed better resistance to deterioration from light and moisture [37].

At the SnO_2/perovskite interface, the usage of a 3-aminopropyltriethoxysilane (APTES) layer as a passivation layer has also been investigated [38]. The electron transport layer (ETL) surface is covered with dipoles to the terminal functional groups of APTES, which also modify the work function of SnO_2. In a word, the energy band offsets must therefore be modified by interface engineering in order to produce highly efficient and reliable perovskite solar cells (PSCs).

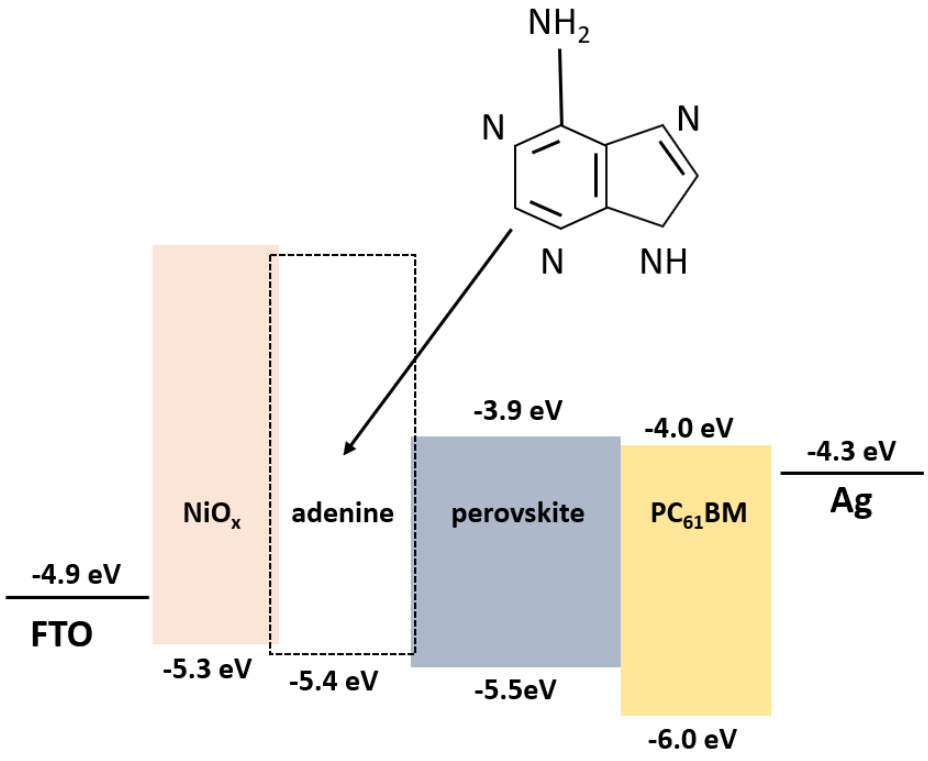

Figure 2.8: The use of adenine as interface modifier, the inset shows the molecular structure of adenine (adapted from Fig. 1b of ref 37)

2.9.3 Interfacial Charge Dynamics

The performance of the device is significantly impacted by the charge dynamics processes that take place at the interfaces in perovskite solar cells (PSCs). These processes may include photogenerated charge extraction, charge transfer, and charge recombination. Deep-level imperfections at interfaces have the potential to cause carrier recombination and a loss of open-circuit voltage (V_{oc}). To improve V_{oc} in PSCs, it is essential to reduce charge recombination at interfaces. Furthermore, high carrier mobility in ETL/HTL is important for facilitating interfacial charge dynamics.

The establishment of a built-in electric field that promotes charge separation and directs electrons and holes towards opposing interfaces is known as interface modification [39]. By utilising interface dipoles, interlayers with functional groups and high conductivity can encourage favourable charge dynamics at interfaces and reduce carrier losses. The introduction of graphene ink into low-temperature processed SnO_2 lowered charge recombination and considerably increased the electron extraction efficiency [40]. Controlled electron affinity molecules have also been used to modify the HTL/perovskite interface in inverted PSCs, where the ability to extract holes from the interface is frequently difficult. The molecules are able to significantly alter the conductivity of HTL, improving the V_{oc} and FF, which leads to an outstanding PCE of 22.1% [41].

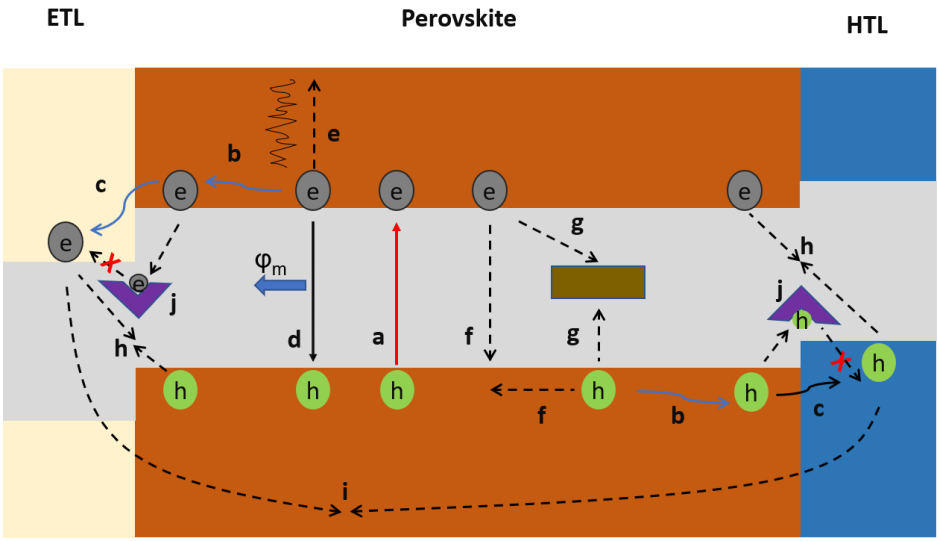

Figure 2.9: Charge transfer and recombination processes in a perovskite solar cell: a) photoexcitation of the perovskite to generate free carriers (holes and electrons); b) diffusion of charge; c) injection of photogenerated electrons into ETL and holes into HTL; d) radiative decay leading to photoluminescence at interface e) auger recombination; f) bimolecular recombination; g) trap-assisted nonradiative monomolecular recombination h) back charge transfer at CTL/PVK interface; i) nonradiative charge recombination at direct contact between ETL and HTL interface; j) surface recombination caused by trap states at interface and grain boundaries (adapted from Fig.5 of ref 39)

2.10 Scopes of Interface Modification

Interface engineering is essential in enhancing the efficiency of perovskite solar cells (PSCs) as it can alter the interface states for charge transport and collection. Numerous researchers have investigated how interface engineering could improve device performance, and their findings offer insightful information about the possibility for advancement. Interface engineering can be applied in Electrode/ETL, ETL/Perovskite, Perovskite/HTL and HTL/Electrode interfaces.

2.10.1 Electrode/ETL Interface

The electron-transporting layer (ETL) and the metal electrode often have a considerable energy level mismatch in inverted structure perovskite solar cells (PSCs). This difference may obstruct effective electron extraction and reduce overall efficiency. Researchers have looked into practical interfacial adjustments at the ETL and electrode interface to solve this problem.

Liu et al. looked into the use of isatin and a derivative of it as an interface layer to lessen the density of interface traps. Performance increased as a result of this adjustment [42]. The layer improved the interface contact, improving electron transport and extraction by passivating surface flaws. The layer had high thermal stability and served as a protective capping layer, preventing deterioration brought on by oxygen and moisture.

2.10.2 ETL/Perovskite Interface

The interface between the electron transport layer (ETL) and the perovskite layer is crucial for electron extraction and injection, defect passivation, energy level alignment, and device stability in perovskite solar cells (PSCs). Additionally, this interface significantly affects the morphology of perovskite films in PSCs with normal structures and prevents hole transmission in PSCs with inverted structures. Numerous methods have been used to alter the ETL/perovskite interface to enhance the performance and stability of the device which are disucussed in this context.

2.10.2.1 Metal Oxides

Metals oxieds are populer as ETLs due to their suitable band alignment, good charge mobility, low cost, and long-term stability in perovskite solar cells (PSCs). Among these, TiO_2 has been being used as ETL for a long time because of a wide bandgap to reduce parasitic absorption, the right

conduction band alignment with the perovskite for effective electron injection, and outstanding electron transport properties. TiO_2 does, however, have several limitations when used as an ETL in PSCs. It has UV-induced photocatalytic activity which may lower device efficiency. Additionally, TiO_2 ETLs can be a factor in capacitance-related problems that lead to current-voltage (I-V) hysteresis, and TiO_2 deposition frequently needs high processing temperatures above 450 °C. Other metal oxides with broad bandgaps, such as MgO, Al_2O_3, ZrO_2, and SnO_2, have been used to reduce charge recombination at the TiO_2/perovskite interface in order to overcome these difficulties [43].

In comparison to conventional TiO_2 ETLs, SnO_2 electron transport layers (ETLs) have attracted a lot of attention for use in perovskite solar cells (PSCs). Notably, SnO_2 outperforms TiO_2 in a number of crucial ways. The first benefit is that it can be treated at lower temperatures, which lowers the energy needed for fabrication. Second, compared to TiO_2, SnO_2 ETLs have lower current-voltage (I-V) hysteresis, which enhances overall device performance. Additionally, SnO_2 exhibits enhanced photostability and lacks photocatalytic activity, making PSCs made with SnO_2 ETLs extremely stable under visible-light illumination, particularly when UV light is present [44]. The SnO_2 ETL serves as an encapsulating layer on top of the perovskite layer in p-i-n type devices, effectively preventing the passage of moisture and oxygen molecules and boosting the long-term stability.

Researchers have investigated numerous interfacial modification techniques to get rid of hysteresis in perovskite solar cells (PSCs). One strategy included addressing the chemical stability restrictions of ZnO-based PSCs by adding a thin layer of MgO at the ZnO/perovskite interface. MgO increased device performance and PSC stability by lowering electron recombination at the interface [45].

Another strategy reduced interfacial losses and modulated energy offsets by using a bilayer electron transport layer (ETL) [46]. For instance, when a SnO_2 amorphous layer was added at the TiO_2/perovskite interface, charge collection was improved, and carrier recombination was reduced. In comparison to a control device, the power conversion efficiency (PCE) was 21.4% with less hysteresis.

Additionally, the bilayer ETL made of In_2O_3 and SnO_2 successfully decreased energy level mismatch and improved charge transfer [47]. The bilayer ETL reduced voltage loss and produced PSCs with a record PCE of 23.2% and exceptional stability by facilitating electron charge transfer from the perovskite to the indium tin oxide (ITO) substrate.

2.10.2.2 Zwitterion

Zwitterionic molecules have covalently bound cations and anions inside the same molecule. These compounds have the amazing ability to create interfacial dipoles, which significantly improves charge injection and extraction in PSCs [48]. Zwitterionic molecules create chemical interactions with the perovskite layer and the electron transport layer (ETL) through their cationic and anionic groups and can passivate the flaws at interfaces.

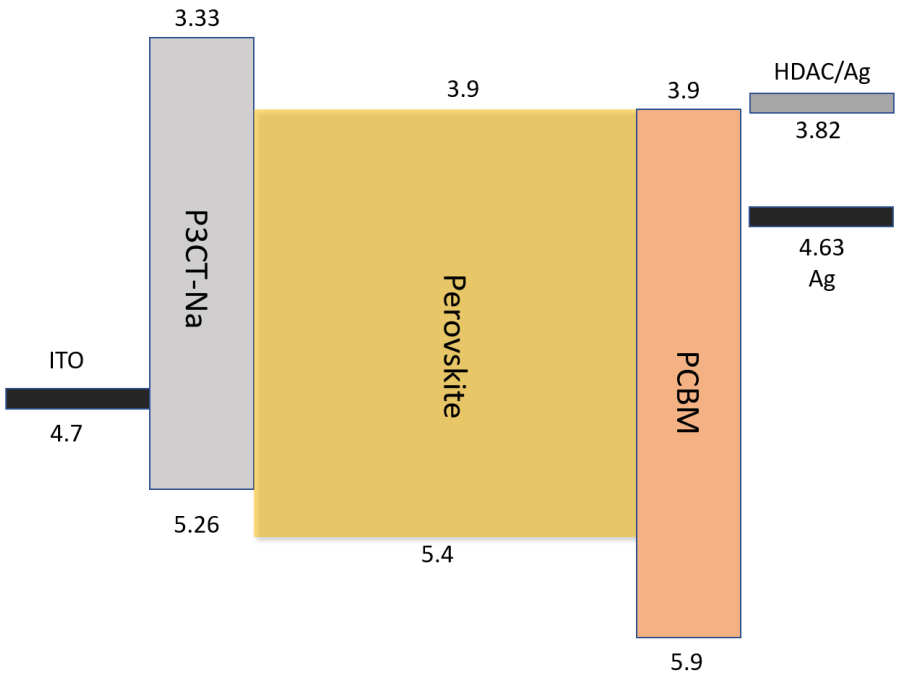

Figure 2.10: Device structure with Zwitterionic molecules (HDAC) (adapted from Fig.6a of ref 48)

SnO_2 has grown its popularity as ETL in perovskite solar cells (PSCs) with a typical planar form in recent years. But due to the problem of hysteresis, planar PSCs often have a lower power conversion efficiency (PCE). Ammonium fluoride (NH_4F) which is a bifunctional zwitterionic molecule, has been used to alter the surface of SnO_2 in order to solve this problem [49]. Through chemical doping, the NH_4F modification decreases defect sites and modifies the energy level of SnO_2 thin films. The adjustment led to a higher PCE of 23.2% and a higher photovoltage of 1.16 V for the PSC device.

In addition, amine silane coupling agent (PASCA-Br) was synthesised and used as a flexible zwitterionic molecular interlayer between the TiO_2 and perovskite layers [50]. This interlayer created solid bonds with the perovskite and TiO_2 layers and reduced the strain at the interface. Additionally, the PASCA-Br interlayer served as a mechanical cushion, lowering the likelihood of

cracks appearing in the perovskite film during bending and enhancing the stability and flexibility of the device.

2.10.2.3 Fullerene Group

Due to favourable electrical characteristics like the strong electron mobility and superior electron-extracting properties of C60 or PCBM ETLs, PSCs using these materials have high fill factor (FF) values and less current-voltage (I-V) hysteresis. The incompatibility of fullerene based ETLs with stable noble metals like Ag is a drawback because of energy misalignment. This problem can be solved by adding interfacial layers between the fullerene (C60 or PCBM) and the metal electrode. This would lower the energy barrier for electron transmission and enhance FF values, particularly for p-i-n type PSCs.

At the ETL/perovskite interface, fullerene and its functionalized derivatives have also been used as surface modifiers. These interface techniques efficiently reduce trap-aided charge recombination, promote device stability, and enable interfacial charge transfer. For instance, the Lewis-acid fullerene skeleton PCBB-3N-3I works well as an interface layer to improve charge collection and decrease trap-assisted recombination, leading to a 21.1% improvement in device performance [51]. Iodide passivates the positive defects on the perovskite surface, which encourages the orientated assembly of PCBB-3N-3I and results in the formation of a dipole layer with an improved interfacial energy band structure.

2.10.2.4 Metal Halides

Device performance and stability can be greatly impacted by the presence of ionic defects at the electron transport layer (ETL)/perovskite interface because they can cause harmful nonradiative

recombination. To solve this problem, interface modification using metal halides with various cations and anions has been used, enabling the simultaneous passivation of cationic and anionic defects at the ETL/perovskite interface. This strategy has been demonstrated to boost long-term stability against light, heat, and moisture while improving device performance.

According to one study [52], a KCl passivation layer could efficiently reduce the interfacial trap density which resulted in an increase in open circuit voltage and litlle hysteresis. Lithium doping was also checked as a way to increase the electron extraction ability of TiO_2. The performance of the device was impacted by the doping of Li-salts onto mp-TiO_2, including LiTFSI, Li_2CO_3, LiCl, and LiF. Deeper conduction bands were produced by Li_2CO_3 doping when compared to other circumstances, yielding a champion power conversion efficiency (PCE) of 25.3% and a verified PCE of 24.7% [53]. The PCE of perovskite solar cells could be further enhanced by optimizing the ETL characteristics.

2.10.3 Perovskite/HTL Interface

The interface between the perovskite layer and the hole transport layer (HTL) is essential for hole extraction and electron blocking. Solution processing technique and high-temperature growth can create ionic vacancies and dangling bonds which results in considerable recombination losses in the film. Additionally, hygroscopic dopants and additives are necessary for commonly used Spiro-OMeTAD as HTL in n-i-p structure PSCs in order to improve their conductivity [54]. These additions might hasten the deterioration of perovskite film. In order to improve hole extraction, passivate flaws, and improve device stability at the perovskite-HTL interface, interlayer materials and techniques have been developed.

2.10.3.1 Organic HTL

The choice of hole transport layers (HTLs) has significant effect on the performance of the perovskite solar cells (PSCs). Spiro-OMeTAD was first used in solid-state DSSCs [55] and is still in use today as HTL. As Spiro-OMeTAD has low conductivity and low hole mobility, dopants and additives like Li-TFSI and tBP must be added for improved performance. Due to their hygroscopic nature, these additions may also introduce instability. As a result, attempts have been made to create dopant-free HTLs as well as novel dopants with increased efficiency and stability [56].

2.10.3.2 Inorganic HTL

Vaious inorganic p-type materials have been investigated as potential substitutes in order to address the stability issues related to organic hole-transporting layers (HTLs) in perovskite solar cells (PSCs). Out of these materials, NiO has received the most attention as a p-type HTL because of its advantageous characteristics including a wide bandgap, high transmittance, and a deep valence band [57].

Another good option for HTL is Copper thiocyanate (CuSCN) which has a deep valence band, strong carrier mobility, good thermal stability, and great transparency [58]. CuSCN is ideal for both p-i-n and n-i-p type devices since it is soluble in a variety of solvents and does not require a post-annealing step for crystallisation. But it has been found that during annealing, the CuSCN HTL in p-i-n devices may interact with the perovskite layer. This interaction can result in performance deterioration [59].

Copper oxide (CuO_x) has also been checked as an HTL material in PSCs as it has deep valence band and high carrier mobility. $CuGaO_2$-based HTLs have demonstrated promising performance in p-i-n devices, particularly when combined with a NiO HTL with Zn-doped and bi-layered

structures [60]. A conversion efficiency of 18.51% was attained by n-i-p devices using undoped $CuGaO_2$ HTL that was directly deposited over the perovskite layer. These devices also showed remarkable long-term stability in ambient settings.

2.10.3.3 Metal Salts

Metal salts can create strong chemical connections with the perovskite surface which can prevent ion migration and guard against the loss of unstable components. The perovskite material is extremely well protected from harsh environmental factors like humidity or light irradiation when metal salts are used as interface layers [61]. Metal salts have been used as interface layers in a small number of publications, but their effects are clear, demonstrating their promise as an effective interfacial material for PSCs.

2.10.3.4 Polymers

Insulating polymers have been found to improve both device stability and the reduction of defect-induced recombination at the perovskite/HTL interface. Long molecule chains and a stable barrier of these interface layers improve V_{oc}. The insulating polymer interface layer must be thin to facilitate effective hole extraction. For instance, PMMA has been used to optimize the perovskite/HTL interface and control the crystal development of the perovskite film. Peng et al. reduced interface recombination with better operating voltages, and a high PCE of 20.8% with a stunning V_{oc} of 1.22 V and low hysteresis by incorporating ultrathin PMMA sheets at the bottom surface of the perovskite film [62].

Inverted p-i-n PSCs can also use insulating polymers to change the perovskite/HTL contact. Zhang et al. placed thin insulating polymer films (PMMA or PS) at the HTL/perovskite interface, resulting in an enhanced PCE without hysteresis and a better V_{oc} without significantly changing

the fill factor [63]. This method successfully stopped current leakage and interfacial recombination.

Furthermore, the stability of PSCs can be improved by using insulating polymer interface layers. Kim et al. examined the effect of the interface layers between a hydrophobic and hygroscopic polymer on the environmental stability of PSCs with typical structures. In comparison to PS, they discovered that PEO at the perovskite interface lowered the density of trap states on the perovskite surface [64]. Additionally, the hygroscopic PEO prevented water molecules from penetrating into the perovskite coating by absorbing them, increasing operating stability in high-humidity settings. These results emphasize the function of insulating polymers as interface modification layers and offer a broad strategy for improving PSC stability.

2.10.3.5 Organic Salts

Insulating organic ammonium salts can be useful in passivating flaws and enhancing device performance without the need for a 2D perovskite interfacial layer. Chemical bonding allows ammonium salt-based interface layers to passivate both negatively and positively charged ionic defects. Their dipole moments and dielectric properties also help to lessen carrier recombination. It is important to pick an ammonium salt that has the right chemical groups and is difficult to develop into low-dimensional perovskites. Using appropriate ammonium salts for interface modification has resulted in several noteworthy improvements and validated high PCE values [65].

2.10.4 HTL/Electrode Interface

Perovskite solar cells (PSCs) can degrade in performance over time, despite encapsulation and dry surroundings. The interaction of Iodine ions with the Silver from electrode at the HTL/electrode contact can result in undesired deterioration. Additionally, positive bias and continuous light illumination worsen Au/Ag ion migration and diffusion that can lower the PCE of PSCs.

Researchers have investigated several interfacial barriers between the HTL and metal electrode in order to solve these problems and to improve device stability [66].

Interlayers between the HTL and electrode have also been made of inorganic metallic oxides. Yang et al [67] tried a structure with gold nano-mesh with MoO_3 layers. This layer improved both optical transparency and conductivity. The top MoO_3 layer reduced reflection at the gold layer which in turn enhanced the performance of the device. Although certain approaches have been investigated, there is still a dearth of knowledge on the HTL/electrode interface, making more optimization in this area necessary.

2.11 Summary

Many significant issues that are related to the thesis have been discussed in this chapter. In addition to introducing the commonly used terms related to perovskite solar cell, various techniques for improving the solar cell performance are also discussed with previous experimental results to understand the device architecture and working principle properly.

CHAPTER 3: THEORETICAL MODEL

3.1 Introduction

Halide perovskite solar cells (PSCs), which are among the most promising solar cells, have attracted a lot of attention recently. This is mainly because of their steadily increasing power conversion efficiency, the affordability of the photovoltaic materials, the simplicity of their manufacturing methods, and their compatibility with flexible substrates. Within a very short span of time, the power conversion efficiency (PCE) of PSCs has increased greatly from 3.8% in 2009 [1] to 25.5% at present [2]. Due to their exceptional intrinsic features, including a long exciton diffusion length, outstanding crystallinity, strong charge carrier mobility, capacity to assist bipolar transport, and longer charge carrier diffusion length, perovskites have achieved high performance in PSC devices.

There are mainly three perovskite halides used in photovoltaic solar cells such as, methylammonium lead triiodide ($MAPbI_3$, where MA is CH_3NH_3), mixed halide $MAPbI_{3-x}Cl_x$, and Formamidinium based $(FAPbI_3)_x(MAPbBr_3)_{1-x}$, where FA is NH_2CHNH_2. $MAPbI_3$ can be doped with Cl to make $MAPbI_{3-x}\,Cl_x$, which is a more stable perovskite [68]. The perovskite $(FAPbI_3)_{0.85}\ (MAPbBr_3)_{0.15}$ shows a stable perovskite phase. The polycrystalline form of these perovskites still shows good charge transport properties. The hole drift mobility is slightly better than electron drift mobility (the drift mobility varies from 2 to 20 $cm^2V^{-1}s^{-1}$) [69, 70]. The usual perovskite photovoltaic structure consists of a bulk perovskite layer that is sandwiched between two thin electron and hole transport layers (ETL and HTL layers). These very thin ETL and HTL layers are the interfacial layers between the bulk perovskite layer and the contact electrodes and

act as n and p-type layers, respectively. Therefore, the photovoltaic structure is equivalent to p-i-n or n-i-p type [71, 72].

Though PSCs show high PCE in a single cell, the cell network must show a stable current-voltage (J-V) characteristics over a long-term operation [73]. Therefore, systemic research is essential to understand the efficiency limiting factors to improve their performance further. A limited number of previous publications proposed mathematical models for explaining the J-V characteristics of perovskite solar cells [4, 74] but didn't consider the explicit effects of surface recombination, which plays a very significant role on the photocurrent and power conversion efficiency (PCE) [51, 75]. Since the built-in electric field is not very strong p-i-n or n-i-p type photovoltaic structures, the charge carrier diffusion, and bulk and surface recombination play significant role on the charge carrier transport, and hence on both the dark and photocurrent (i.e., the current-voltage characteristics depends on both the dark and photocurrent).

In this thesis, a comprehensive mathematical model for the current-voltage characteristics in perovskite solar cell is developed by considering charge carrier diffusion along with bulk and surface recombination. The air mass (AM) 1.5 global spectrum is specifically used to represent the incident sun radiation. The continuity equation for both holes and electrons are solved to determine the electron and hole profiles. The position dependent total conduction current (sum of the drift and diffusion currents of both holes and electrons) under steady state condition is calculated and compared with the total photocurrent calculated using the Shockley-Ramo's theorem. The theoretical model is used to explain the reasons for the variation of experimental results with the variation of cell material compositions by comparing the theoretical results with the experimental data. The important carrier transport and cell properties can be extracted from these comparisons.

3.2 Mathematical Theory

The photons of incident sunlight are absorbed in the bulk heterojunction perovskite layer with an exponential distribution, which create free electron–hole pairs (EHPs) over the whole perovskite layer. The EHP generation rate *G* is, [76]

$$G(\lambda, x) = G_0(\lambda)\,\mathrm{e}^{-\alpha(\lambda)x} \tag{3.1}$$

And

$$G_0(\lambda, 0) = \alpha\lambda I_0 / hc \tag{3.2}$$

where λ is the wavelength of the incident photon, x is the distance from the radiation-receiving electrode (i.e., the top contact), the EHP carrier generation rate at $x = 0$ is denoted as G_0, α is the absorption coefficient of the perovskite, I_0 is the intensity of the solar radiation, h is the Plank constant and c is the speed of light.

The photogenerated electrons and holes move under both drift and diffusion processes. In a p-i-n type structure, holes drift towards the radiation-receiving contact and electrons drift towards the bottom contact (their drifting directions in a p-i-n structure are the opposite of that in a n-i-p). Few assumptions are made to allow the carrier dynamics to be analytically tractable [77]: (1) A uniform built-in electric field F across the bulk perovskite layer under small signal analysis, and (2) a constant drift mobility (μ) and a single lifetime (τ) of holes and electrons in the active layer. It was shown that the electric field distribution throughout the absorber layer is almost uniform if the layer thickness is less than a micrometer [78]. In fact, the active perovskite layer thickness of the cells is usually ~0.5 μm.

The continuity equations for holes and electrons in the perovskite layer under steady-state are (assuming that the electrons are drifting towards the radiation-receiving electrode):

$$\frac{\partial}{\partial t}(\delta_p) = D_p \frac{\partial^2}{\partial x^2}(\delta_p) - \mu_p F \frac{\partial}{\partial x}(\delta_p) + Ge^{-\alpha(\lambda)x} - \frac{\delta_p}{\tau_p} = 0 \quad \textbf{(3.3)}$$

$$\frac{\partial}{\partial t}(\delta_n) = D_n \frac{\partial^2}{\partial x^2}(\delta_n) + \mu_n F \frac{\partial}{\partial x}(\delta_n) + Ge^{-\alpha(\lambda)x} - \frac{\delta_n}{\tau_n} = 0 \quad \textbf{(3.4)}$$

where δ_n (δ_p), τ_n (τ_p), μ_n (μ_p), D_n (D_p) are the concentrations of photogenerated excess electrons (holes), average electron (hole) lifetime, drift mobility of electrons (holes), and diffusion coefficient of electrons (holes), respectively.

Considering, the particular solution for equation (3): $\delta_p(x) = A_1 e^{-\alpha(\lambda)x}$ and by substituting in equation (3) , we can find A_1 where,

$$A_1 = \frac{G\tau_p}{1 - \mu_p F \alpha \tau_p - D_p \alpha^2 \tau_p} \quad \textbf{(3.5)}$$

In the same way, from equation (4) we can find A_2 where,

$$A_2 = \frac{G\tau_n}{1 + \mu_n F \alpha \tau_n - D_n \alpha^2 \tau_n} \quad \textbf{(3.6)}$$

Since ETL and HTL layers are very thin and much more conductive than the bulk layer, the amount of voltage drop in these two layers is negligible, the external voltage-dependent electric field F in the perovskite layer can be approximated as

$$F \approx \frac{V_{bi} - (V - JR_s)}{W} \quad \textbf{(3.7)}$$

where V is the load voltage, J is the net current in the external circuit, V_{bi} is the built-in potential, W is the thickness of the perovskite layer and R_s is the effective series resistance including the current path through the ETL and HTL transport layers.

If the conduction photocurrent densities are J_n and J_p due to electron and hole movements, respectively; the current densities can be characterized by the following expressions:

$$J_p(x) = q\mu_p F\delta_p(x) - qD_p \frac{\partial}{\partial x}\delta_p(x) \quad \textbf{(3.8)}$$

$$J_n(x) = q\mu_n F\delta_n(x) + qD_n \frac{\partial}{\partial x}\delta_n(x) \quad \textbf{(3.9)}$$

Where q is the elementary charge. The concentration of defect states at the two interfaces of the perovskite layer is much higher than the bulk layer and thus the current density at the interface is determined by the surface recombination current, which is characterised by the surface recombination velocity S. At the interfaces, the current density can be characterized by the following equation [5],

$$q\mu_p F\delta_p(x) - qD_p \frac{\partial}{\partial x}\delta_p(x) = -qS_p\delta_p(x) \quad \textbf{(3.10)}$$

$$q\mu_n F\delta_n(x) + qD_n \frac{\partial}{\partial x}\delta_n(x) = qS_n\delta_n(x) \quad \textbf{(3.11)}$$

Using these boundary conditions in both interfaces, the solutions of the equations (3) and (4) are:

$$\delta_p(x,\lambda) = C_1 e^{m_1 x} + C_2 e^{m_2 x} + A_1 e^{-\alpha x} \quad \textbf{(3.12)}$$

$$\delta_n(x,\lambda) = C_3 e^{m_3 x} + C_4 e^{m_4 x} + A_2 e^{-\alpha x} \quad \textbf{(3.13)}$$

respectively. The value of m_1,m_2, m_3 & m_4 can be determined from the characteristic solution of equations (3) and (4) where,

$$m_1 = \frac{\mu_p F + \sqrt{\mu_p{}^2 F^2 + 4\frac{D_p}{\tau_p}}}{2D_p}, \qquad m_2 = \frac{\mu_p F - \sqrt{\mu_p{}^2 F^2 + 4\frac{D_p}{\tau_p}}}{2D_p},$$

$$m_3 = \frac{-\mu_n F + \sqrt{\mu_n{}^2 F^2 + 4\frac{D_n}{\tau_n}}}{2D_n}, \qquad m_4 = \frac{-\mu_n F - \sqrt{\mu_n{}^2 F^2 + 4\frac{D_n}{\tau_n}}}{2D_n}$$

Applying boundary condition at x=0 and x=W using equation (10) and (11) and solving for C_1, C_2, C_3 and C_4 we can find:

$$C_1 = \frac{A_1(\alpha D_p + \mu_p F + S_P)(e^{-\alpha W} - e^{m_2 W})}{(D_p m_1 - \mu_p F - S_P)(e^{m_1 W} - e^{m_2 W})}, \qquad C_2 = \frac{A_1(\alpha D_p + \mu_p F + S_P)(e^{m_1 W} - e^{-\alpha W})}{(D_p m_2 - \mu_p F - S_P)(e^{m_1 W} - e^{m_2 W})},$$

$$C_3 = \frac{A_2(\mu_n F - S_n - \alpha D_n)(e^{m_4 W} - e^{-\alpha W})}{(D_n m_3 + \mu_n F - S_n)(e^{m_3 W} - e^{m_4 W})}, \qquad C_4 = \frac{A_2(\mu_n F - S_n - \alpha D_n)(e^{-\alpha W} - e^{m_3 W})}{(D_n m_4 + \mu_n F - S_n)(e^{m_3 W} - e^{m_4 W})},$$

Substituting the excess carrier profiles from (9) and (10) into equations (6) and (7), the position dependent hole and electron photocurrents are:

$$J_p(x) = qD_p[m_1 C_2 e^{m_2 x} + m_2 C_1 e^{m_1 x} + A_1 e^{-\alpha x}(m_1 + m_2 + \alpha)] \quad \textbf{(3.14)}$$

$$J_n(x) = -qD_n[m_3 C_4 e^{m_4 x} + m_4 C_3 e^{m_3 x} + A_2 e^{-\alpha x}(m_3 + m_4 + \alpha)] \quad \textbf{(3.15)}$$

And the total photocurrent,

$$J_{ph}(\lambda, V) = J_n(x) + J_p(x) \quad \textbf{(3.16)}$$

Under steady state condition, the total photocurrent in equation (16) should be space-invariant. Alternatively, the induced photocurrent can also be calculated using the Shockley–Ramo theorem [79, 80]. Using this theorem, the photocurrent for the incident photon of wavelength λ is,

$$J_{ph}(\lambda, V) = \frac{q}{W}[\{\mu_p F \int_0^W \delta_p \partial x - D_p \int_0^W \frac{\partial \delta_p}{\partial x} \partial x\} + \{\mu_n F \int_0^W \delta_n \partial x + D_n \int_0^W \frac{\partial \delta_n}{\partial x} \partial x\}]$$

$$= \frac{q}{W}[\mu_p F\{\frac{C_1}{m_1}(e^{m_1 W}-1)+\frac{C_2}{m_2}(e^{m_2 W}-1)-\frac{A_1}{\alpha}(e^{-\alpha W}-1)\}$$
$$-D_p\{C_1(e^{m_1 W}-1)+C_1(e^{m_2 W}-1)+A_1(e^{-\alpha W}-1)\}$$
$$+\mu_n F\{\frac{C_3}{m_3}(e^{m_3 W}-1)+\frac{C_4}{m_4}(e^{m_4 W}-1)-\frac{A_2}{\alpha}(e^{-\alpha W}-1)\}$$
$$+D_n\{C_3(e^{m_3 W}-1)+C_4(e^{m_4 W}-1)+A_2(e^{-\alpha W}-1)\}] \quad \textbf{(3.17)}$$

The resultant photocurrent density for the entire sun spectra can be written as,

$$J_{ph}(V)=\int_0^{\infty} J_{ph}(\lambda, V)d\lambda \quad \textbf{(3.18)}$$

The net external current density from a solar cell under an external load can be written as, [12, 81]

$$J(V)=J_d(V)+\frac{V-R_s J(V)}{R_p}-J_{ph}(V), \quad \textbf{(3.19)}$$

where $J_d(V)$ is the dark current density and R_p is the shunt area resistance. The mathematical expression dark current can be written as [74, 82]

$$J_d = J_c \frac{V_t}{V_{bi}-(V-JR_s)}\times\{\exp(\frac{V-JR_s}{2V_t})-\exp[\frac{2(V-JR_s)-V_{bi}}{2V_t}]\} \quad \textbf{(3.20)}$$

And
$$J_c \approx qn_i W[\frac{1}{\tau_n}\exp(\frac{\varphi_p-\varphi_n}{2V_t})+\frac{1}{\tau_p}\exp(\frac{\varphi_n-\varphi_p}{2V_t})] \quad \textbf{(3.21)}$$

where the intrinsic carrier concentration in the perovskite layer is denoted as n_i, V_t the thermal voltage, ($V_t = k_b T/q$, where T is the temperature and k_b is the Boltzmann constant), φ_n and φ_p are the effective barrier heights for electrons and holes, respectively.

3.3 Summary

In this chapter, the necessary theoretical model is developed by solving the steady state continuity equation for photogenerated carrier. The proper boundary conditions for including the effect of surface and bulk recombination are also determined which will be used in next chapter to show the effect of these parameters in the photocurrent and overall efficiency.

CHAPTER 4: RESULTS AND DISCUSSION

4.1 Introduction

In the previous chapter, the theoretical model was shown for calculating total photocurrent. It was possible to simplify the model under some certain conditions. The thickness of the active perovskite layer is considered ~0.5 μm. The incident photon flux $I_0(\lambda)$ is considered as the air mass (AM) 1.5 global spectrum [83]. The mobility-lifetime products of electrons and holes in perovskite materials are quite comparable (within one order of magnitude) [84]. For simplicity, both electron and hole mobility-lifetimes are assumed to be equal in the theoretical calculations of this paper. Since the EHP generation profile is exponential across the perovskite layer and attenuation depth (i.e., $1/\alpha$) is small compared to W, the carrier type (electrons or holes) that moves towards the bottom electrode controls the charge collection efficiency. The other type of carriers contributes very little to the photocurrent. Therefore, the mentioned values of the mobility-lifetimes mainly represent for the carrier type that drifts toward the bottom electrode.

Using the software MATLAB, the photogenerated carrier concentrations and corresponding photo current were plotted to analyze the effect of different parameters. The effects of carrier mobility, lifetime and surface recombination effect on carrier concentration and total photo current were shown graphically. Finally, the model was verified by fitting the theoretical results with published experimental data.

4.2 Effect of Surface Recombination Velocity

The following figures show the photogenerated charge carrier concentration profiles across the perovskite layer in an ITO/PTAA/$MAPbI_3$/PCBM/C60/BCP/Cu structure as a function of surface recombination velocity.

The structure is a p-i-n type where PTAA and PCBM act as hole and electron transport layers, respectively. The assumed physical parameters are [74]; $R_s = 5\,\Omega.cm^2$, $R_p > 10^4\ \Omega.cm^2$, , J_c =3.048 × 10^{-12} Acm^{-2}, and $\mu\tau$ = 5.6×10^{-6} $cm^2\,V^{-1}$ and $S_n = S_p$ = 50 ms^{-1} . As mentioned earlier, in p-i-n structure, the photogenerated holes travel towards radiation receiving interface (top surface) resulting in highest hole concentration in HTL-perovskite interface and lowest in ETL- perovskite interface which is depicted in **Figure 4.1**.

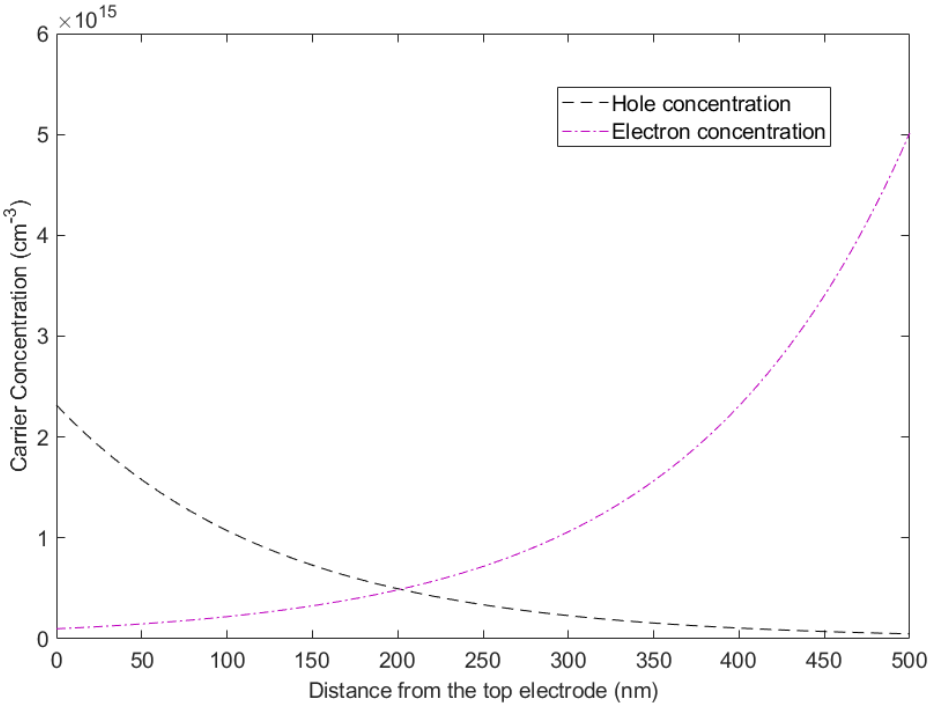

Figure 4.1: The photogenerated carrier concentration profile across the perovskite layer in a p-i-n type structure as a function of distance from the top electrode, x

Similarly, the photogenerated electrons travel towards the ETL-perovskite interface in the bottom resulting in highest concentration in the bottom interface. The profile distribution of the two carriers is opposite over the perovskite layer as expected.

As mentioned above, due to the built-in field in the active layer, the photo-generated holes immediately start drifting towards the top contact and recombine with a velocity of S_p (surface recombination velocity) at the interfacial layer between the perovskite and the top contact. In the same way, electrons immediately start drifting towards the bottom contact and recombine with a velocity of S_n at the interfacial layer between the perovskite and the bottom contact. The surface recombination velocity highly depends on the charge carrier concentrations at the very thin interfacial layers. Again, higher surface recombination velocity results in lower carrier concentration at the interfaces (perovskite/ETL or HTL/perovskite) which in turn affect the total current density and overall power conversion efficiency.

To observe the effect of surface recombination velocity in carrier distribution over the structure, the value of surface recombination is varied within an acceptable range keeping other parameters constant for the same p-i-n structure and resultant effects were plotted in **Figure 4.2.**

For hole $\mu\tau = 5.6\times10^{-6}$ cm^2 V^{-1} and $S_p = 50$ ms^{-1}, the corresponding hole profile distribution is shown. The maximum concentration at HTL-perovskite interface is found as 2.32×10^{15} cm^{-3} where the minimum concentration at perovskite-ETL interface is 4.94×10^{13} cm^{-3}.

With the same transport parameter for electron with $\mu\tau = 5.6\times10^{-6}$ cm^2 V^{-1} and $S_n = 50$ ms^{-1} , the corresponding electron profile distribution is shown in the same figure. The minimum concentration at HTL-perovskite interface is found as 9.96×10^{13} cm^{-3} where the maximum concentration at perovskite-ETL interface is 5.01×10^{15} cm^{-3}.

Keeping the same transport parameters $\mu\tau$ = 5.6×10^{-6} cm^2 V^{-1} and changing S_p to 100 ms^{-1} for hole, the maximum concentration at HTL-perovskite interface is found as 1.34×10^{15} cm^{-3} where the minimum concentration at perovskite-ETL interface is 2.89×10^{13} cm^{-3}. With the same identical parameters for electron $\mu\tau$ = 5.6×10^{-6} cm^2 V^{-1} and S_n = 100 ms^{-1}, the minimum concentration at HTL-perovskite interface is found as 3.51×10^{13} cm^{-3} where the maximum concentration at perovskite-ETL interface is 1.93×10^{15} cm^{-3}.

For much higher S_p = 200 ms^{-1} and same $\mu\tau$ = 5.6×10^{-6} cm^2 V^{-1} for hole, the corresponding hole profile distribution plot gives the maximum concentration at HTL-perovskite interface as 7.27×10^{14} cm^{-3} where the minimum concentration at perovskite-ETL interface is found 1.61×10^{13} cm^{-3}.

For electron $\mu\tau$ = 5.6×10^{-6} cm^2 V^{-1} and S_n = 200 ms^{-1}, the corresponding electron profile distribution shows the minimum concentration at HTL-perovskite interface as 1.27×10^{13} cm^{-3} where the maximum concentration at perovskite-ETL interface is found to be 8.66×10^{14} cm^{-3}.

The summarized effect of surface recombination on both hole and electron's surface concentration is shown in **Figure 4.2**. It is evident that surface concentration reduces for both electron and hole with the increment of surface recombination velocity.

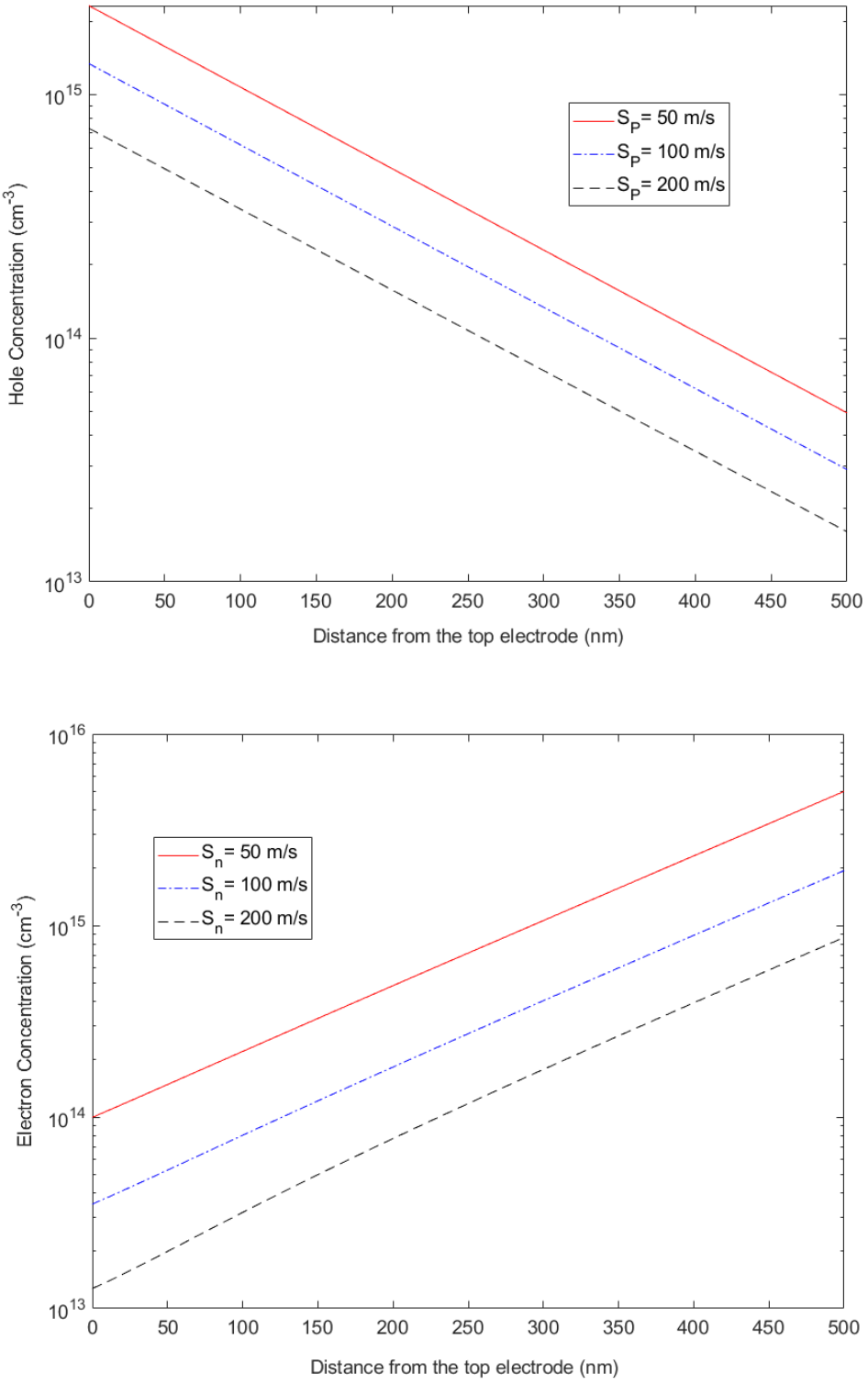

Figure 4.2: The photogenerated charge carrier concentration profiles across the perovskite layer in a p-i-n type structure as a function of surface recombination velocity

The effect of surface recombination of carriers on the overall power conversion efficiency (PCE) of the above-mentioned perovskite solar cell is shown in **Figure 4.3**. The surface recombination velocity for both hole and electron are considered equal. The physical parameters in the mathematical model for **Figure 4.3** are the same as for **Figure 4.1**. The PCE efficiency decreases with increasing surface recombination. To get the optimal efficiency, the surface recombination velocity should be as low as possible.

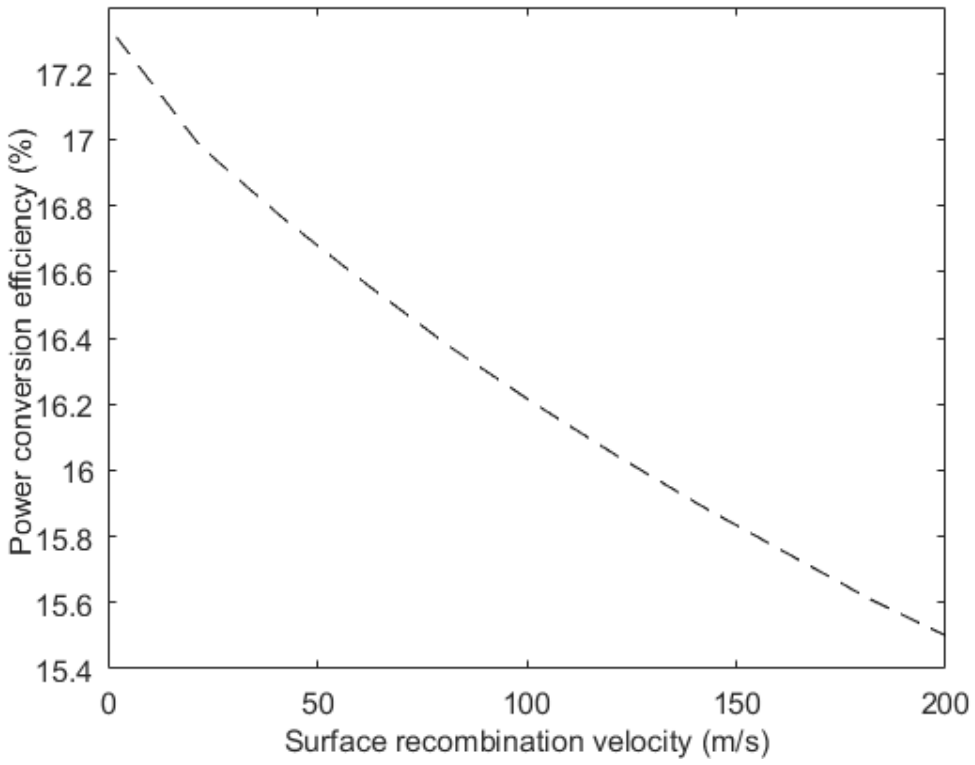

Figure 4.3: The effect of surface recombination velocity on the power conversion efficiency (PCE) of a $MAPBI_3$ based solar cell

To observe the change of carrier profile over the structure with enhanced carrier transport, the value of $\mu\tau$ is varied up to 10 times keeping $S_n = S_p = 50$ ms^{-1} for the same p-i-n structure and resultant effects were plotted in **Figure 4.4.**

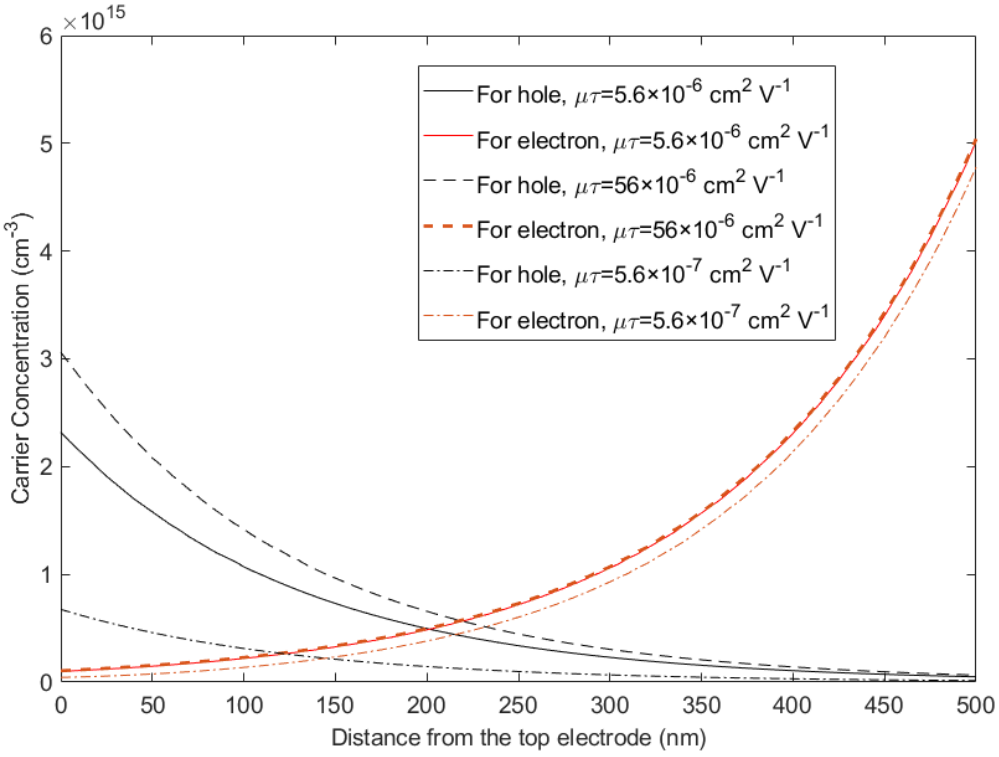

Figure 4.4: The photogenerated carrier concentration profile across the perovskite layer in a p-i-n type structure as a function of distance from the top electrode, x. Here μτ is varied from μτ= 5.6×10^{-7} cm^2 V^{-1} to μτ=56×10^{-6} cm^2 V^{-1} for both hole and electron.

For hole $\mu\tau = 5.6\times10^{-6}$ cm^2 V^{-1} and $S_p = 50$ ms^{-1}, the maximum concentration at HTL-perovskite interface is found as 2.32×10^{15} cm^{-3} where the minimum concentration at perovskite-ETL interface is 4.94×10^{13} cm^{-3}. For the equal parameters for electron, the minimum concentration at HTL-perovskite interface is found as 9.96×10^{13} cm^{-3} where the maximum concentration at perovskite-ETL interface is 5.01×10^{15} cm^{-3}.

With Increased $\mu\tau$ = 56×10^{-6} cm^2 V^{-1} and same S_p = 50 ms^{-1} for hole, the maximum concentration at HTL-perovskite interface is found as 3.06×10^{15} cm^{-3} where the minimum concentration at perovskite-ETL interface is 6.52×10^{13} cm^{-3}. For electron, the minimum concentration at HTL-perovskite interface is found as 1.05×10^{14} cm^{-3} where the maximum concentration at perovskite-ETL interface is 5.04×10^{15} cm^{-3} with $\mu\tau$ = 56×10^{-6} cm^2 V^{-1} and Sn = 50 ms^{-1}

Reducing the hole $\mu\tau$ to 5.6×10^{-7} cm^2 V^{-1} with S_p = 50 ms^{-1}, there is a reduction on surface concentration with the maximum concentration at HTL-perovskite interface of 6.75×10^{14} cm^{-3} and the minimum concentration at perovskite-ETL interface of 1.44×10^{13} cm^{-3}. Following the same trend, for electron $\mu\tau$ = 5.6×10^{-7} cm^2 V^{-1} and S_n = 50 ms^{-1}, the corresponding electron profile the minimum concentration at HTL-perovskite interface is reduced to 4.37×10^{13} cm^{-3} with the maximum concentration at perovskite-ETL interface of 4.77×10^{15} cm^{-3}.

The photocurrent density across the perovskite layer for $S_P = S_n$ = in the same p-i-n type structure is shown in **Figure 4.5**. The sum of electron and hole current is constant, which is equal to J_{ph} = 24.6 mA/cm^2 while the $\mu\tau$ of both hole and electrons are considered equal as 5.6×10^{-6} cm^2 V^{-1} s^{-1}. The total current can also be calculated using the Shockley-Ramo's theorem (equation (15)), which gives the same value of photocurrent, (J_{ph} = 24.6 mA/cm^2). Therefore, under-steady condition, the conduction current (equation (14)) is equal to the total photocurrent current as described by the Shockley-Ramo's theorem.

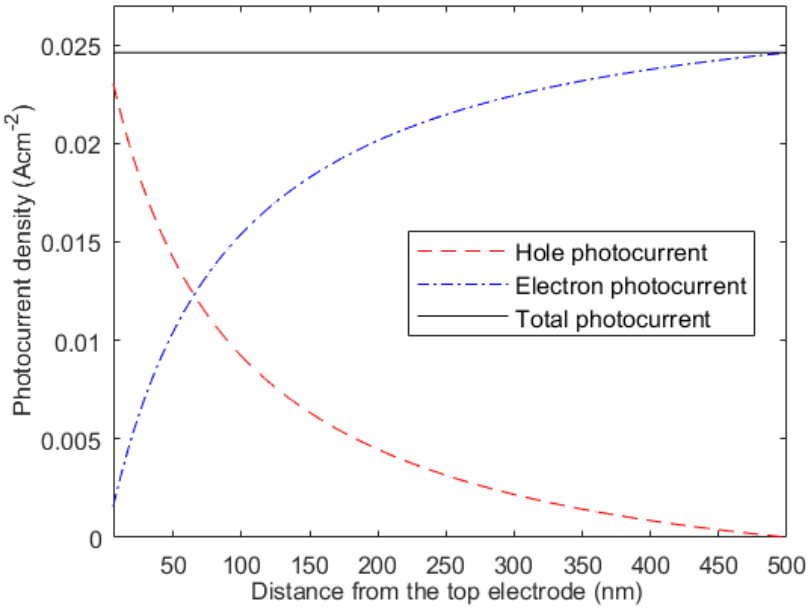

Figure 4.5: Photocurrent densities as a function of distance, x from the top electrode

To observe the effects of transport parameter i.e., the μτ product is varied keeping the same surface recombination for both hole and electron. There is no change in total photocurrent for the change of hole lifetime τ_p up to 10 times as holes are going to the top contact. The same total photocurrent $J_{ph} = 24.6$ mA/cm^2 is found which is shown in **Figure 4.6**. Although, electrons are going to bottom electrode, there is no change in total current with the change of electron lifetime τ_n up to 10 times which is expected for a very short channel device.

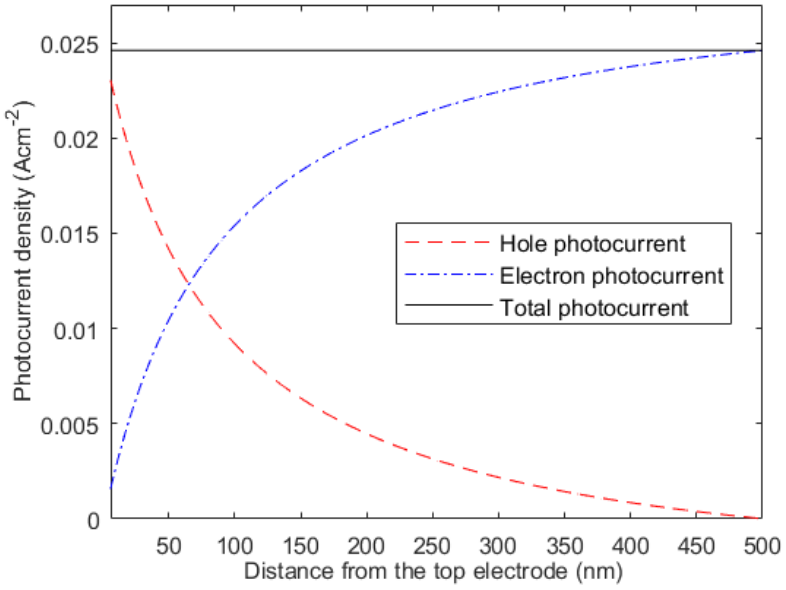

Figure 4.6: Photocurrent densities as a function of distance, x from the top electrode where $\mu\tau=56\times10^{-6}$ cm^2 V^{-1} for hole

The change of total current with the change of mobility for both hole and electron were also observed. For hole, there was no change with the change of hole mobility μ_p from 4 cm^2 V^{-1} s^{-1} to 16 cm^2 V^{-1} s^{-1} produced the same total photocurrent of J_{ph} = 24.6 mA/cm^2.

The change of total photocurrent is found for bottom going carrier (electron for p-i-n structure) when the μ_n is changed within an acceptable range for the same perovskite structure. The corresponding results are shown in following **Figure 4.7 & 4.8**.

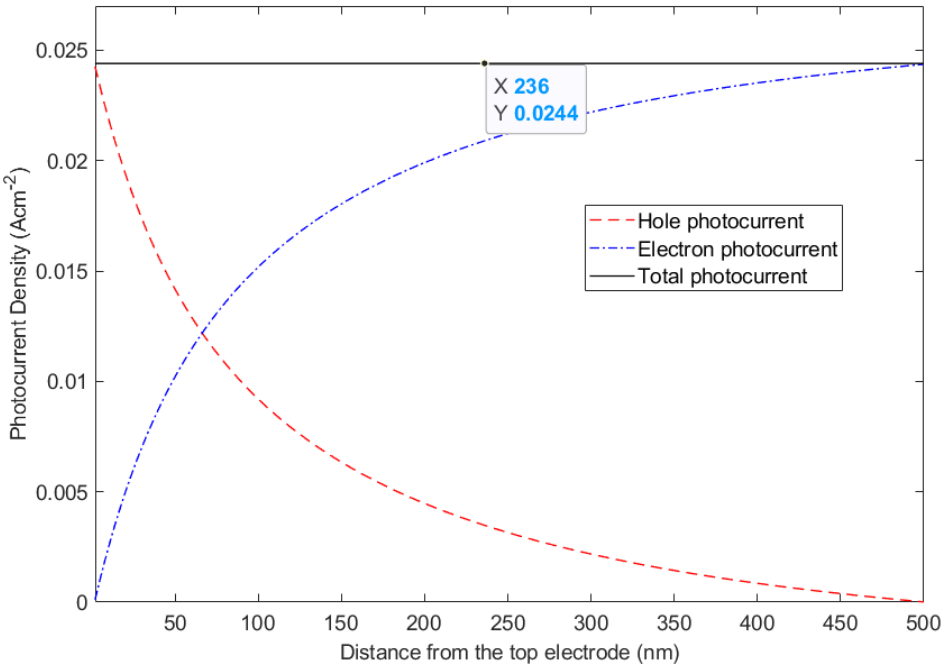

Figure 4.7: Photocurrent densities as a function of distance, x from the top electrode where μ=4 cm^2 V^{-1} for electron.

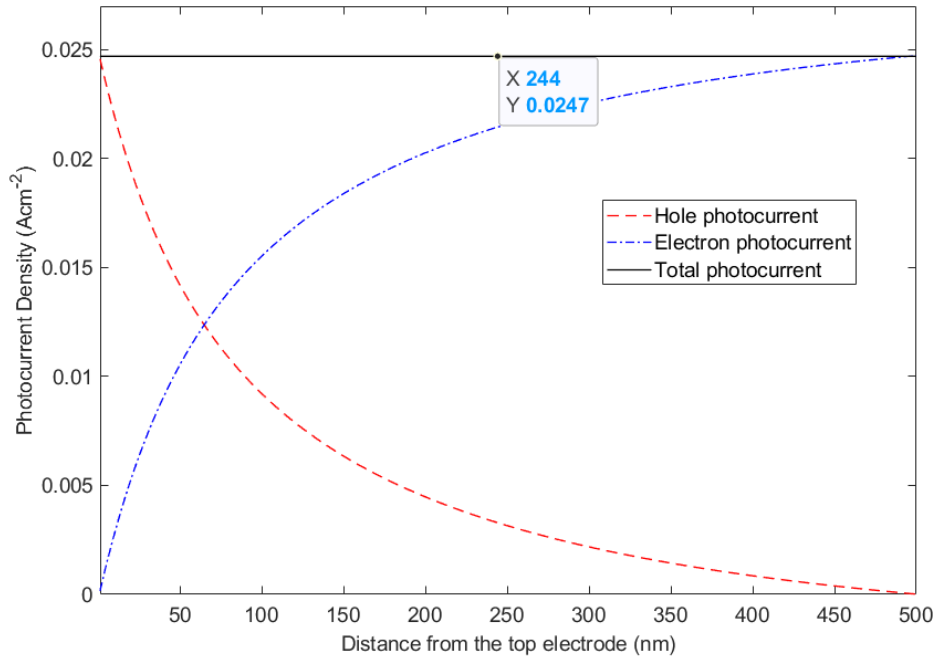

Figure 4.8: Photocurrent densities as a function of distance, x from the top electrode where μ=16 cm^2 V^{-1} s^{-1} for electron.

To identify the effect of surface recombination solely, the $\mu\tau$ kept constant for both hole and electron as $\mu\tau = 5.6\times10^{-6}$ cm^2 V^{-1} s^{-1} and the surface velocity is varied within an acceptable range. The change in total photocurrent is seen when the surface velocity of the bottom going carrier (electron for PIN structure) is varied. For $S_p = 2\times10^4$ cms^{-1} and $S_n = 2\times10^5$ cms^{-1}, the total photocurrent reduces to $J_{ph} = 23.4$ mA/cm^2 as shown in **Figure 4.9**.

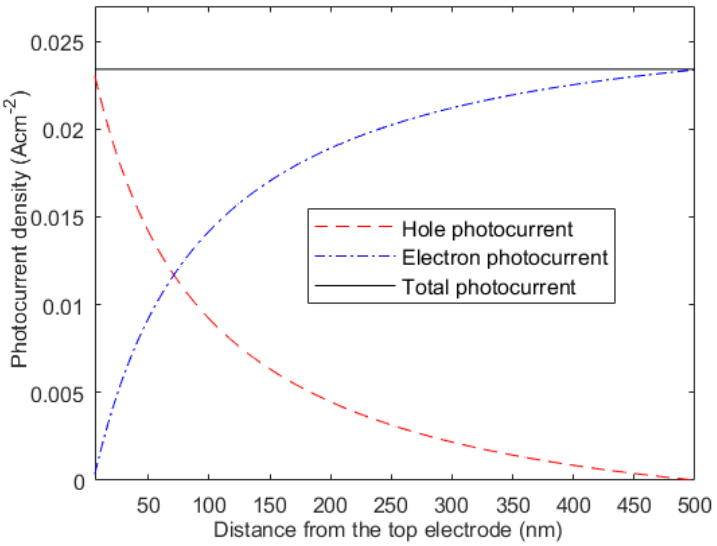

Figure 4.9: Photocurrent densities as a function of distance, x from the top electrode. Here S_n is increased up to 10 times to observe surface recombination effect on device performance.

For $S_p = 2\times10^4$ cms^{-1} and $S_n = 2\times10^3$ cms^{-1}, the total photocurrent increases to $J_{ph} = 24.9$ mA/cm^2 as shown in **Figure 4.10**.

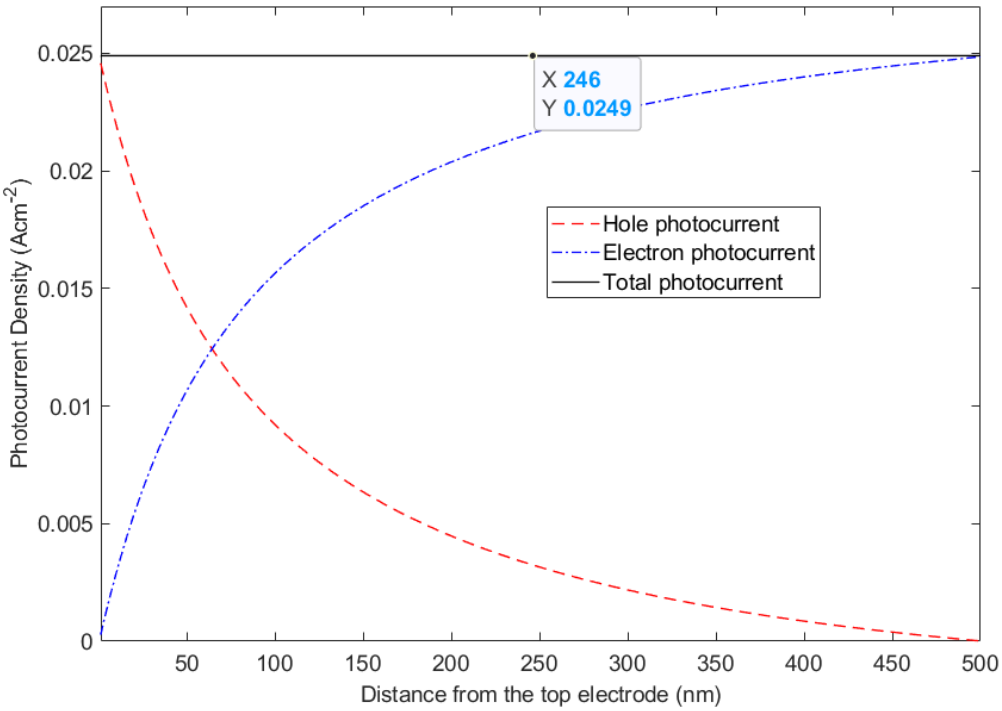

Figure 4.10: Photocurrent densities as a function of distance, x from the top electrode. Here S_n is reduced up to 10 times to observe surface recombination effect on device performance.

The current remains same for changing the surface velocity up to 10 times for the carrier (Hole for PIN structure here) that is going to top contact, as expected. For $S_p = 2\times10^3$ cms^{-1} and $S_n = 2\times10^4$ cms^{-1}, the total photocurrent is same as J_{ph} = 24.6 mA/cm^2 as found previously which is shown in **Figure 4.11**.

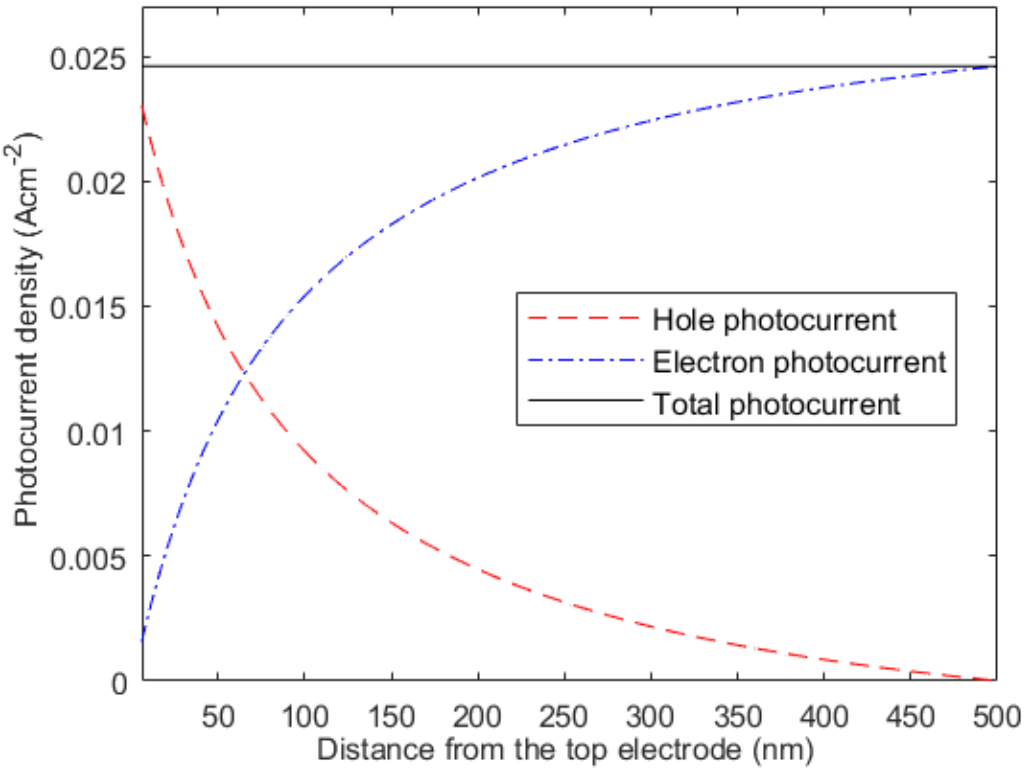

Figure 4.11: Photocurrent densities as a function of distance, x from the top electrode. Here S_p is reduced up to 10 times to observe surface recombination effect on device performance.

As described above, the surface recombination velocity has a very significant effect on the free carrier concentrations and so does on the photocurrent and overall power conversion efficiency. For all the cases, the total photocurrent calculated from the model remains equal to the current calculated with Shockley-Ramo's theorem which validates the model.

4.3 Model fitting with Experimental Results:

In this section the proposed analytical model is applied to various types of perovskite solar cells and the physical reasons for the deviations of current-voltage characteristics with varying material

compositions are explained by comparing the model with the published experimental data. The current–voltage characteristics of the ITO/PTAA/$MAPbI_3$/PCBM/C60/BCP/Cu solar cell with varying PCBM (ETL) layer are shown in **Figure 4.12**. Three types of ETL layers such as with PCBB-3N, without PCBB-3N and with PCBB-3N-3I interlayer are examined with a perovskite layer thickness of 0.3 µm, ITO layer thickness of 0.12 µm and Cu electrode of 0.1 µm. The solid line and symbols represent the model fit and the extracted experimental data results for three different ETL layer compositions from Figure 1 of [51]. The extracted physical parameters for all three structures are given in Table 1.

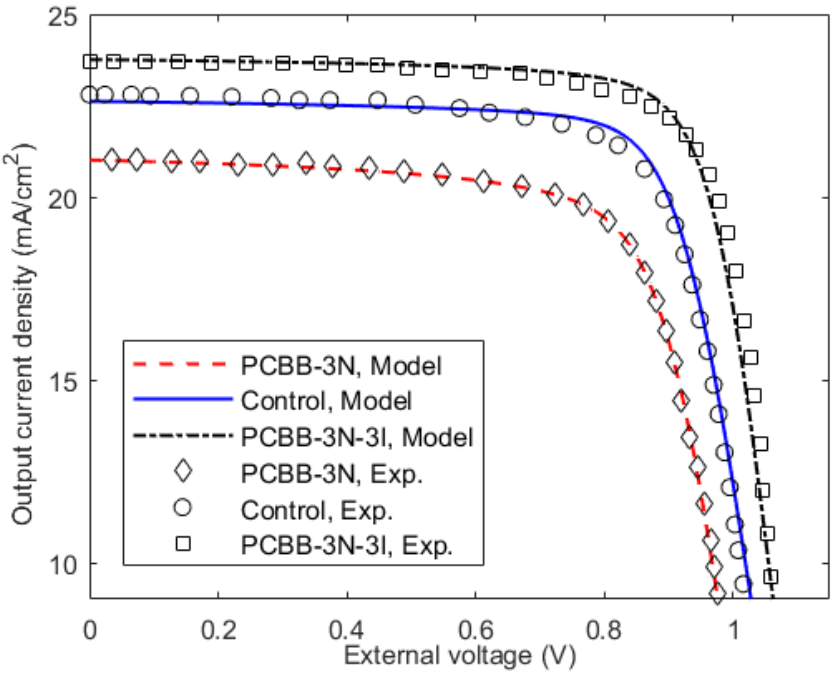

Figure 4.12: Current-voltage characteristics of an ITO/PTAA/MAPbI3/PCBM/C60/BCP/Cu $MAPbI_3$-based solar cell. Here Exp. stands for the extracted experimental data from [51].

The theoretical model shows a very good agreement with the experimental results. The fitting parameters show a better charge carrier transport properties with PCBB-3N-3I interlayer structure (ITO/PTAA/$MAPbI_3$ /PCBB-3N-3I/PCBM/C60/BCP/Cu) resulting in a PCE=19.75 % higher than the basic control device (without any interlayer at perovskite/ETL interface) having PCE=17.84%.

By addressing charged surface defects and altering the energy band structure at the interface by adding a fullerene electrolyte (PCBB-3N-3I) dipole interlayer between the perovskite active layer and the ETL, the power conversion efficiency is increased. This result shows a strong likelihood that after iodide ionisation, coating the perovskite active layer with a fullerene skeleton with Lewis's acid can simultaneously decrease trap-assisted recombination and increase the built-in voltage (V_{bi}) and charge collection efficiency.

Figure 4.13 shows the J-V curves of $FAMAPbI_3$-based cells having different interfacial material [85] for the ETL layer. The compositions of the three structures are ITO/In_2O_3/$FAMAPbI_3$ /spiro/Au, ITO/SnO_2/$FAMAPbI_3$/spiro/Au, and ITO/In_2O_3/SnO_2/$FAMAPbI_3$/spiro/Au. The extracted physical parameters for the three structures with perovskite layer thickness of 0.7 μm, ETL thickness of 0.03 μm and HTL thickness of 0.2 μm are given in Table 1.

Reduced trap densities, improved energy alignment, and increased charge transfer are the advantages of using a bilayer of In_2O_3 and SnO_2 for the ETL layer. The addition of a bi-layer electron transport layer (ETL) structure improves the transport characteristics of charge carriers, as shown by the higher open circuit voltage and increased PCE values (from 19.16 % to 22.39 %). An ETL made of In_2O_3 and SnO_2 reduces the mismatch in energy band levels, increasing the built-in potential and electric field needed for efficient carrier separation.

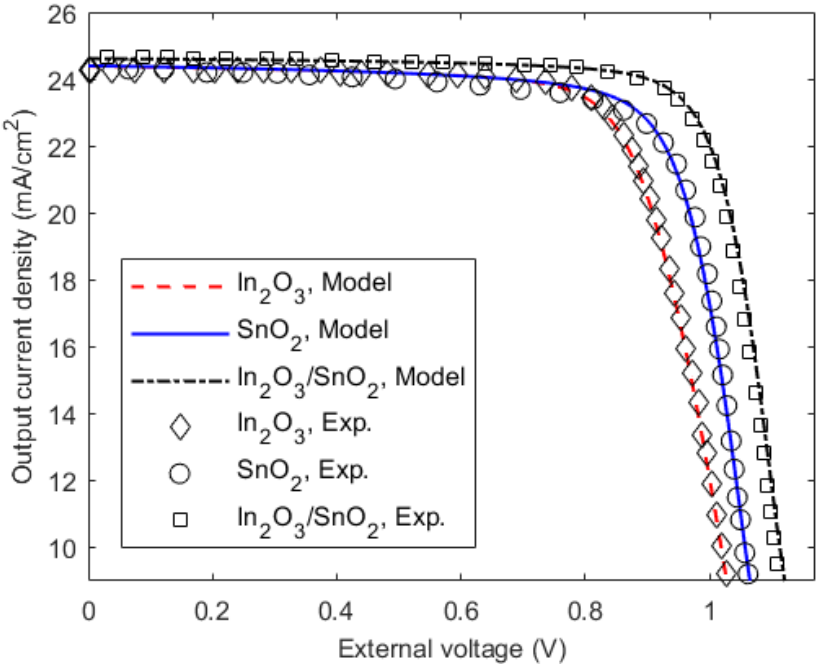

Figure 4.13: The current−voltage characteristics of FAPbI3-based solar cells having different interfacial materials for the ETL layer. Exp. stands for the extracted experimental data from [85]

The J-V characteristics of $Cs_{0.05}(FA_{0.83}MA_{0.17})_{0.95}Pb(I_{0.83}\ Br_{0.17})_3$ based solar cell with n-i-p structure are described in **Figure 4.14**. The composition of the structure is ITO/TiO_2(TiO_2/ APTES/PASCA-Br)/ $Cs_{0.05}(FA_{0.83}MA_{\ 0.17})_{0.95}Pb(I_{0.83}\ Br_{0.17\ })_3$/PCBM/Ag [86]. The symbols and solid lines represent the published experimental data and the model fit to the experimental results of different compositional structures by changing the interfacial material at ETL/perovskite interface. The extracted physical parameters along with a perovskite layer of 0.4 µm, TiO_2 layer of 0.1 µm and Ag electrode of 0.1 µm for the three structures are given in Table 1. The thin interface layer of PASCA-Br with TIO2 based ETL gives improved carrier transport properties. By reducing interface strain and lattice distortion, a higher open circuit voltage (V_{oc}) of 1.10 V and a significant increase in PCE of 17.80% are made possible.

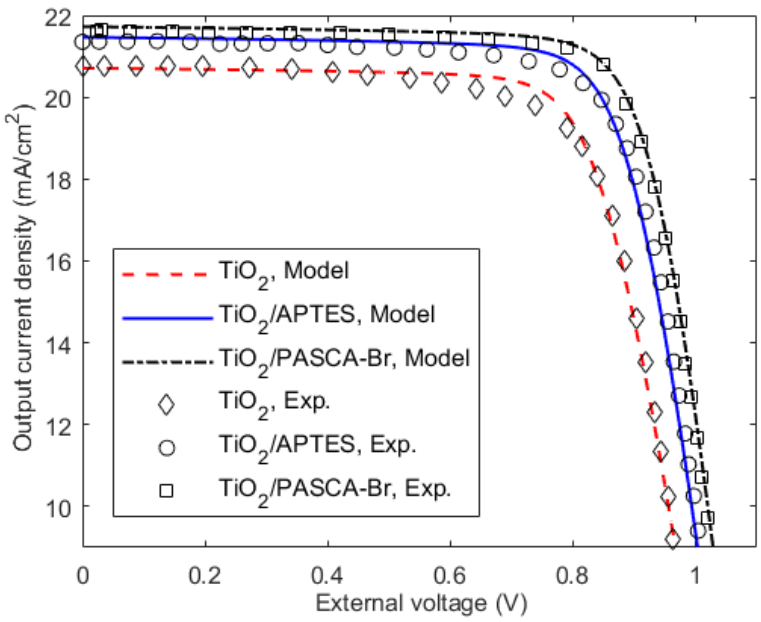

Figure 4.14: Current−voltage characteristics of a $Cs_{0.05}(FA_{0.83}MA_{0.17})_{0.95}Pb(I_{0.83}Br_{0.17})_3$-based solar cell. Exp. stands for the extracted experimental data from [86]

The current–voltage characteristics of ITO/SnO_2/$(FAPbI_3)_x(MAPbBr_3)_{1-x}$/SpiroOMeTAD/Ag based solar cells are shown in **Figure 4.15**. To improve the device performance, theophylline or caffeine was used as an interfacial material between HTL/perovskite interface [75]. The extracted physical parameters for the three structures are given in Table 1 while the perovskite layer thickness used is 0.7 µm where HTL thickness used is 0.3 µm with Ag electrode of 0.6 µm. The targeted device showed improved carrier transport properties, leading to a higher open circuit voltage (V_{oc}) of 1.19 V and a better PCE of 23.10% by using intermolecular interactions to passivate flaws in the perovskite material.

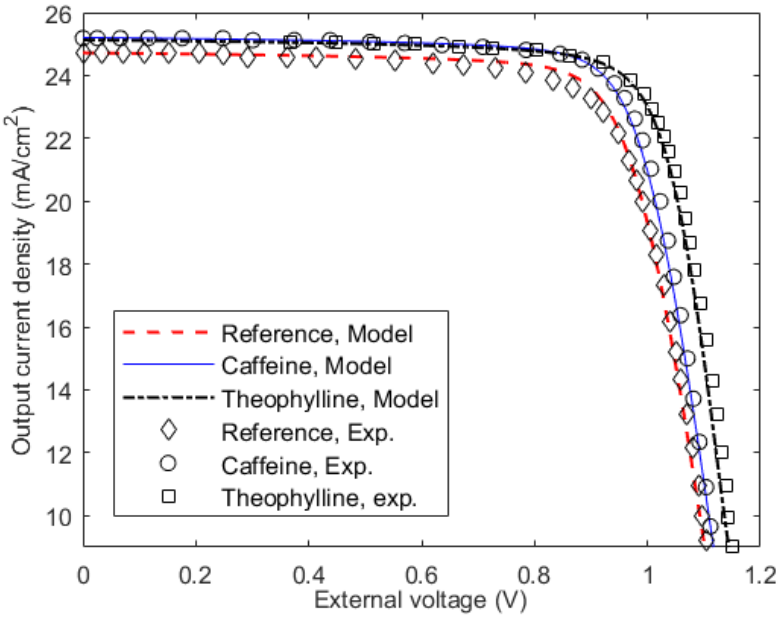

Figure 4.15: Current−voltage characteristics of a $(FAPbI_3)_{0.92}(MAPbBr_3)_{0.8}$ based solar cell. Exp. stands for the extracted experimental data from [75].

Table 4.1: The fitting parameters for figures 4.12 to 4.15. $R_p > 10^4$ Ω.cm^2 in all cases and its effect is negligible.

Cell Material	**ETL/HTL with/without Treatment**	V_{bi} **(V)**	J_c **(A/cm^2)**	R_s **(Ω .cm^2)**	$\mu\tau$ **(cm^2/V)**	$S_p = S_n$ **(cm/s)**	**PCE (%)**
$MAPbI_3$ [51]	PCBB-3N	1.03	3.20×10^{-11}	6	3.2×10^{-7}	1.3×10^{4}	15.42
	Control (without interlayer)	1.06	2.85×10^{-11}	5.5	3.6×10^{-7}	1.25×10^{4}	17.84
	PCBB-3N-3I	1.10	1.61×10^{-11}	4	1.6×10^{-6}	1.15×10^{4}	19.75
$FAMAPbI_3$ [85]	In_2O_3	1.10	2.49×10^{-11}	6.5	9.6×10^{-7}	4×10^{3}	19.16
	SnO_2	1.12	1.99×10^{-11}	3.8	1.2×10^{-6}	3.8×10^{3}	20.51
	In_2O_3/SnO_2	1.16	9.13×10^{-12}	3	4.5×10^{-6}	3.6×10^{3}	22.39
	TIO_2	1.04	4.3×10^{-11}	7	3.2×10^{-7}	3.2×10^{3}	15.50

$Cs_{0.05}(FA_{0.83}MA_{0.17})_{0.95}Pb(I_{0.83}Br_{0.17})_3$ [86]	TIO_2/APTES	1.08	3.4×10^{-11}	6.5	4×10^{-7}	3×10^{3}	16.93
	TIO_2/PASCA-Br	1.10	2.84×10^{-11}	5.5	4.8×10^{-7}	2.9×10^{3}	17.80
$(FAPbI_3)_{0.92}(MAPbBr_3)_{0.8}$ [75]	Reference Control (without interlayer)	1.16	5.98×10^{-12}	6	4×10^{-6}	3×10^{3}	21.33
	Caffeine interlayer	1.17	4.97×10^{-12}	5.5	4.8×10^{-6}	2.9×10^{3}	22.19
	Theophylline interlayer	1.19	4.6×10^{-12}	3.8	5.2×10^{-6}	2.8×10^{3}	23.10

4.4 Summary

The theoretical model results are discussed and analyzed in this chapter. The carrier concentration and photo-current over the layer thickness (distance from the top contact) with varying mobility-lifetime products are plotted to understand the bulk recombination effect. The surface recombination is also varied to understand the effect of it on photogenerated hole and electron distribution, photocurrent and overall efficiency and corresponding results are also analyzed and plotted. Finally, the theoretical outcomes are matched with previously released experimental data in order to verify the mathematical models and the extracted parameters are finally shown in a Tabular format.

CHAPTER 5: CONCLUSION, CONTRIBUTION AND FUTURE WORKS

5.1 Conclusion

This study proposes a concise physics-based mathematical model that explains the effects of bulk and surface recombination on the external voltage-dependent photocurrent in various perovskite solar cells. Theoretical calculations and experimental results from several perovskite solar cells have been compared to validate the theoretical model. Excellent agreement has been found between the model and experimental data, demonstrating the models' value in predicting carrier transport and cell characteristics. The concise physics-based analytical model described in this paper can be used to derive crucial carrier transport and cell parameters for enhancing the power conversion efficiency of perovskite, organic and other thin-film solar cells.

5.2 Contribution

A part of this work has been submitted for peer reviewed journal publication; Sheikh M. Shuvoraj and M. Z. Kabir, “Current–Voltage Characteristics of Perovskite Solar Cells Incorporating Bulk and Surface Recombination: Comparison of a Physics-Based Model Calculations with Experiments”, Journal of Material Science: Materials in Electronics (asked for minor revision and it is in the process of submitting the revised version).

5.3 Future Works

The thesis provides a model created exclusively for perovskite solar cells, but with some essential modifications, it may be modified and verified for usage in other thin film solar cells. Since the efficiency of the solar cell significantly depends on the optical and electrical properties of the components that make up the active layer, improving the performance of photovoltaic devices can be accomplished through the design of materials. Additionally, in order to reduce the consequences of surface recombination, it is crucial to find and use the best interface engineering.

A thorough physics-based model is provided in this thesis to analyze the effects of various regulating factors on the current-voltage characteristics. This study will therefore be a useful tool for creating solar cells with the highest efficiency. The existence of a constant electric field throughout the active layer is a key premise of this argument. Therefore, it is essential to develop a mathematical model that take variable electric fields within the active layers into account. The active layer is also treated as neutral in this thesis, despite the possibility of pre-existing carriers brought on by doping, which might drastically change the total current computation. Future research in this thesis may look into analyzing these consequences.

REFERENCES

1 A. Kojima, K. Teshima, Y. Shirai, T. Miyasaka, Organometal Halide Perovskites as Visible Light Sensitizers for Photovoltaic Cells*, J. Am. Chem. Soc.,* vol 131, 6050−6051, 2009

2 H. Min, D.Y. Lee, J. Kim, G. Kim, K.S. Lee, J. Kim, M.J. Paik, Y.K. Kim, K.S. Kim, M.G. Kim, T.J. Shin, S.I. Seok, Perovskite solar cells with atomically coherent interlayers on SnO_2 electrodes, *Nature,* vol 598, pp. 444-450, 2021

3 J. Young Kim, J. Wook Lee, H. Suk Jung, H. Shin, and N. Park, High-Efficiency Perovskite Solar Cells, *Chem. Rev.,* vol 120, pp. 7867-7918, 2020

4 T. S. Sherkar, C. Momblona, L. Gil-Escrig, H. J. Bolink, L. J. A. Koster, Improving Perovskite Solar Cells: Insights From a Validated Device Model, *Adv. Energy Mater,* vol 7, 1602432, 2017

5 X. Sun, R. Asadpour, W. Nie, A. D. Mohite, M. A. Alam, A Physics-Based Analytical Model for Perovskite Solar Cells, *IEEE J. Photovoltaics,* vol 5, 1389-1394, 2015

6 D. Bi, W. Tress, M.I. Dar,P. Gao,J Luo, C. Renevier, K. Schenk, A. Abate, F. Giordano, J. P. C. Baena, J. D. Decoppet, S. M. Zakeeruddin, M. K. Nazeeruddin, M. Gratzel, A. Hagfeldt, Efficient luminescent solar cells based on tailored mixed-cation perovskites, *Sci. Adv.,* vol 2, 1501170, 2016

7 M.A. Green, A. H. Baillie, H. J. Snaith , The emergence of perovskite solar cells, *Nature Photonics*, vol 8, 506–514, 2014

8 Wikipedia. Available online: https://en.wikipedia.org/wiki/Perovskite_(structure) (accessed on 6 October 2023)

9 F. Wang, Y. Cao, C. Chen, Q. Chen, X. Wu, X. Li, T. Qin, W. Huang, Materials toward the Upscaling of Perovskite Solar Cells: Progress, Challenges, and Strategies, *Advanced Functional Material,* vol 28 issue 52, 2018

10 N. Marinova, S. Valero, J. L. Delgado, Organic and perovskite solar cells: Working principles, materials and interfaces, *Journal of Colloid and Interface Science,* vol 488, 373-389, 2017

11 O. Gunawan, S. R. Pae, D. M. Bishop, Y. Virgus, J. H. Noh, N. J. Jeon, Y.S. Lee, X. Shao, T. Todorov, D.B. Mitzi & B. Shin ,Carrier-resolved photo-Hall effect, *Nature*, vol 575,151–155, 2019

12 J. Nelson, The Physics of Solar Cells; *Imperial College Press:* London, UK, 2003

13 J. Cubas , S. Pindado, C. de Manuel, Explicit Expressions for Solar Panel Equivalent Circuit Parameters Based on Analytical Formulation and the Lambert W-Function, *Energies ,* vol 7, 4098-4115, 2014

14 T. Markvart, L. Castañer, McEvoy's Handbook of Photovoltaics (Third Edition), *Fundamentals and Applications,* 29-57, 2018

15 Juan Bisquert, The physics of solar cells : perovskites, organics, and photovoltaic fundamentals, CRC Press, Taylor & Francis Group, (2018)

16 M.B Johnston, L.M. Herz, Hybrid Perovskites for Photovoltaics: Charge-Carrier Recombination, Diffusion, and Radiative Efficiencies, *Acc. Chem. Res.,* vol 49, 146-154, 2016

17 A. Amat, E. Mosconi, E. Ronca, C. Quarti, P. Umari, M. K. Nazeeruddin, M. Gratzel, F. D. Angelis, Cation-induced band-gap tuning in organohalide perovskites: interplay of spin-orbit coupling and octahedra tilting, *Nano Lett,* vol 14(6), 3608-16, 2014

18 L.M Herz, Charge-Carrier Mobilities in Metal Halide Perovskites: Fundamental Mechanisms and Limits, *ACS Energy Lett.*, vol 2, 1539−1548, 2017

19 G. E. Eperon, S. D. Stranks, C. Menelaou, M. B. Johnston, L. M. Herz, H. J. Snaith, Formamidinium lead trihalide: a broadly tunable perovskite for efficient planar heterojunction solar cells, *Energy Environ. Sci.* , vol 7, 982, 2014

20 J. P. C. Baena, L. Steier, W. Tress, M. Saliba, S. Neutzner, T. Matsui, F. Giordano, T. J. Jacobsson, A. R. Srimath Kandada, S. M. Zakeeruddin, A. Petrozza, A. Abate, M. K. Nazeeruddin, M. Grätzel, A. Hagfeldt, Highly efficient planar perovskite solar cells through band alignment engineering, *Energy Environ. Sci.,* vol 8, 2928-2934, 2015

21 Y. Wu, X. Yang, W. Chen, Y. Yue, M. Cai, F. Xie, E. Bi, A. Islam, L. Han, Perovskite solar cells with 18.21% efficiency and area over 1 cm2 fabricated by heterojunction engineering, *Nat. Energy,* vol 1, 16148, 2016

22 J.W. Lee, D.H. Kim, H.S. Kim, S.W. Seo, S.M. Cho, N.G. Park, Formamidinium and Cesium Hybridization for Photo- and Moisture-Stable Perovskite Solar Cell, *Adv. Energy Mater.,* vol 5, 1501310, 2015

23 Z. Li, M. Yang, J. S. Park, S. H. Wei, J. J. Berry, K. Zhu, Stabilizing Perovskite Structures by Tuning Tolerance Factor: Formation of Formamidinium and Cesium Lead Iodide Solid-State Alloys, *Chem. Mater.,* vol 28, 284−292, 2016

24 H. Tan, A. Jain, O. Voznyy, X. Lan, F. P. García de Arquer, J. Z. Fan, R. Quintero-Bermudez, M. Yuan, B. Zhang, Y. Zhao, F. Fan, P. Li, L. N. Quan, Y. Zhao, Z.H. Lu, Z. Yang, S. Hoogland, E. H. Sargent, Efficient and stable solution-processed planar perovskite solar cells via contact passivation , *Science,* vol 355, 722,2017

25 J. Lu, X. Lin, X. Jiao, T. Gengenbach, A. D. Scully, L. Jiang, B. Tan, J. Sun, B. Li, N. K. Pai, U. Bach, A. N. Simonov, Y.B. Cheng, Interfacial benzenethiol modification facilitates charge transfer and improves stability of cm-sized metal halide perovskite solar cells with up to 20% efficiency ,*Energy Environ. Sci.* , vol 11, 1880, 2018

26 W. Liao, D. Zhao, Y. Yu, C.R. Grice, C. Wang, A.J. Cimaroli, P. Schulz, W. Meng, K. Zhu, R.G. Xiong, Y. Yan, Lead-Free Inverted Planar Formamidinium Tin Triiodide Perovskite Solar Cells Achieving Power Conversion Efficiencies up to 6.22 , *Adv. Mater.,* vol 28, 9333−9340, 2016

27 R. Lin, K. Xiao, Z. Qin, Q. Han, C. Zhang, M. Wei, M.I. Saidaminov, Y. Gao, J. Xu, M. Xiao, et al., Monolithic all-perovskite tandem solar cells with 24.8% efficiency exploiting comproportionating to suppress Sn(II) oxidation in precursor ink, *Nat. Energy*, vol 4, 864−873, 2019

28 G.P. Nagabhushana, R. Shivaramaiah, A. Navrotsky, Direct calorimetric verification of thermodynamic instability of lead halide hybrid perovskites, A. Proc. *Natl. Acad. Sci. U. S.* A., vol 113, 7717−7721, 2016

29 S. Ryu, J. H. Noh, N. J. Jeon, Y. C. Kim, W. S. Yang, J. Seo, S. I. Seok, Voltage output of efficient perovskite solar cells with high open-circuit voltage and fill factor, *Energy Environ. Sci.,* vol 7, 2614, 2014

30 J.H. Noh, S.H. Im, J.H. Heo, T.N. Mandal, S.I. Seok, Chemical management for colorful, efficient, and stable inorganic-organic hybrid nanostructured solar cells, *Nano Lett.,* vol 13, 1764−1769, 2013

31 M. M. Lee, J. Teuscher, T. Miyasaka, T. N. Murakami, H. J. Snaith, Efficient Hybrid Solar Cells Based on Meso-Superstructured Organometal Halide Perovskites, *Science,* vol 338, 643, 2012

32 J. You, Z. Hong, Y. Yang, Q. Chen, M. Cai, T.-B. Song, C.-C. Chen, S. Lu, Y. Liu, H. Zhou, Y. Yang, Low-Temperature Solution-Processed Perovskite Solar Cells with High Efficiency and Flexibility, *ACS Nano,* vol 8, 1674, 2014

33 W. Shockley, H. J. Queisser, The Shockley-Queisser limit, J. Appl. Phys.,vol 32, 510, 1961

34 J. Peng, Y. Wu, W. Ye, D. A. Jacobs, H. Shen, X. Fu, Y. Wan, T. Duong, N. Wu, C. Barugkin, H. T. Nguyen, D. Zhong, J. Li, T. Lu, Y. Liu, M. N. Lockrey, K. J. Weber, K. R. Catchpole, T. P. White, Interface passivation using ultrathin polymer–fullerene films for high-efficiency perovskite solar cells with negligible hysteresis, *Energy Environ. Sci.,* vol 10, 1792, 2017

35 Y. Shao, Z. Xiao, C. Bi, Y. Yuan, J. Huang, Origin and elimination of photocurrent hysteresis by fullerene passivation in $CH_3NH_3PbI_3$ planar heterojunction solar cells, *Nat. Commun.,* vol 5, 5784, 2014

36 B. Zhao, X. Yan, T. Zhang, X. Ma, X. Li, Introduction of Multifunctional Triphenylamino Derivatives at the Perovskite/HTL Interface To Promote Efficiency and Stability of Perovskite Solar Cells, *ACS Appl. Mater. Interfaces,* vol 12, 9300, 2020

37 L. Xie, Z. Cao, J. Wang, A. Wang, S. Wang, Y. Cui, Y. Xiang, X. Niu, F. Hao, L. Ding, Improving energy level alignment by adenine for efficient and stable perovskite solar cells, *Nano Energy,* vol 74, 104846, 2020

38 G. Yang, C. Wang, H. Lei, X. Zheng, P. Qin, L. Xiong, X. Zhao, Y. Yan, G. Fang, Interface engineering in planar perovskite solar cells: energy level alignment, perovskite morphology control and high-performance achievement, *J. Mater. Chem.* A, vol 5, 1658, 2017

39 A. Rajagopal, K. Yao, A. K. Y. Jen, Toward Perovskite Solar Cell Commercialization: A Perspective and Research Roadmap Based on Interfacial Engineering, *Adv. Mater.,* vol 30, 1800455, 2018

40 M. Zhu, W. Liu, W. Ke, L. Xie, P. Dong, F. Hao, Graphene-Modified Tin Dioxide for Efficient Planar Perovskite Solar Cells with Enhanced Electron Extraction and Reduced Hysteresis, *ACS Appl. Mater. Interfaces,* vol 11, 666, 2019

41 P. Ru, E. Bi, Y. Zhang, Y. Wang, W. Kong, Y. Sha, W. Tang, P. Zhang, Y. Wu, W. Chen, X. Yang, H. Chen, L. Han, High Electron Affinity Enables Fast Hole Extraction for Efficient Flexible Inverted Perovskite Solar Cells, *Adv. Energy Mater.,* vol 10, 1903487, 2020.

42 S. Xiong, M. Yuan, J. Yang, J. Song, Q. Bao, Engineering of the Back Contact between PCBM and Metal Electrode for Planar Perovskite Solar Cells with Enhanced Efficiency and Stability, *Adv. Opt. Mater.,* vol 7, 1900542, 2019

43 J. Ma, G. Yang, M. Qin, X. Zheng, H. Lei, C. Chen, Z. Chen, Y. Guo, H. Han, X. Zhao, G. Fang, MgO Nanoparticle Modified Anode for Highly Efficient SnO2-Based Planar Perovskite Solar Cells, *Adv. Sci.,* vol 4, 1700031, 2017.

44 J.A. Christians, P. Schulz, J.S. Tinkham, T.H. Schloemer, S.P. Harvey, B.J. Tremolet de Villers, A. Sellinger, J.J. Berry, J.M. Luther, Tailored interfaces of unencapsulated perovskite solar cells for >1,000 hour operational stability, *Nature Energy,* vol 3, 68−74, 2018

45 J. Cao, B. Wu, R. Chen, Y. Wu, N. Zheng, Efficient, Hysteresis-Free, and Stable Perovskite Solar Cells with ZnO as Electron-Transport Layer: Effect of Surface Passivation, *Adv. Mater.,* vol 30, 1705596, 2018

46 M. M. Tavakoli, P. Yadav, R. Tavakoli, J. Kong, Surface Engineering of TiO2 ETL for Highly Efficient and Hysteresis-Less Planar Perovskite Solar Cell (21.4%) with Enhanced Open-Circuit Voltage and Stability, *Adv. Energy Mater.,* vol 8, 1800794, 2018.

47 P. Wang, R. Li, B. Chen, F. Hou, X. Zhang, Gradient Energy Alignment Engineering for Planar Perovskite Solar Cells with Efficiency Over 23%, *Adv. Mater.,* vol 32, 1905766, 2020.

48 A. Islam, J. Li, M. Pervaiz, Z.-H. Lu, M. Sain, L. Chen, X. Ouyang, Zwitterions for Organic/Perovskite Solar Cells, Light-Emitting Devices, and Lithium Ion Batteries: Recent Progress and Perspectives, *Adv. Energy Mater.,* vol 9, 1803354, 2019

49 E. H. Jung, B. Chen, K. Bertens, M. Vafaie, S. Teale, A. Proppe, Y. Hou, T. Zhu, C. Zheng, E. H. Sargent, Bifunctional Surface Engineering on SnO_2 Reduces Energy Loss in Perovskite Solar Cells, *ACS Energy Lett.* , vol 5, 2796, 2020

50 C.C. Zhang, S. Yuan, Y.-H. Lou, Q.-W. Liu, M. Li, H. Okada, Z.-K. Wang, Perovskite Films with Reduced Interfacial Strains via a Molecular-Level Flexible Interlayer for Photovoltaic Application, *Adv. Mater.,* vol 32, 2001479, 2020

51 M. Zhang, Q. Chen, R. Xue, Y. Zhan, Y. Li et al., Reconfiguration of interfacial energy band structure for high-performance inverted structure perovskite solar cells, *Nat.*

Com., vol 10, 4593, 2019

52 X. Liu, Y. Zhang, L. Shi, Z. Liu, J. Huang, J. S. Yun, Y. Zeng, A. Pu, K. Sun, Z. Hameiri, Exploring Inorganic Binary Alkaline Halide to Passivate Defects in Low-Temperature-Processed Planar-Structure Hybrid Perovskite Solar Cells, *Adv. Energy Mater.,* vol 8, 1800138, 2018

53 K. Minjin, C. In-Woo, C. Seung Ju, S. Ji Won, M. Sung-In, A. Jeong-Ho, J. Yimhyun, A. SeJin, A. Seoung Kyu, K. Gi-Hwan, K. Dong Suk, Enhanced electrical properties of Li-salts doped mesoporous TiO2 in perovskite solar cells, *Joule,* vol 5, 659, 2021

54 A. Erkan, B. Michele, W. Stefaan, Defect and Contact Passivation for Perovskite Solar Cells, *Adv. Mater.,* vol 31, 1900428, 2019

55 U. Bach, D. Lupo, P. Comte, J.E. Moser, F. Weissortel, J. Salbeck, H. Spreitzer, M. Gratzel, Solid-state dye-sensitized mesoporous TiO2 solar cells with high photon-to-electron conversion efficiencies, *Nature,* vol 395, 583−585, 1998

56 T.H. Schloemer, J.A. Christians, J.M. Luther, A. Sellinger, Doping strategies for small molecule organic hole-transport materials: Impacts on perovskite solar cell performance and stability, *Chem. Sci.,* vol 10, 1904−1935, 2019

57 J.Y. Jeng, K.C. Chen, T. Y. Chiang, P. Y. Lin, T.D. Tsai, Y.C. Chang, T.F. Guo, P. Chen, T.C. Wen, Y. J Hsu, Nickel oxide electrode interlayer in $CH_3NH_3PbI_3$ perovskite/PCBM planar-heterojunction hybrid solar cells, *Adv. Mater.,* vol 26, 4107−4113, 2014

58 M. Lyu, J. Chen, N.G. Park, Improvement of efficiency and stability of CuSCN-based inverted perovskite solar cells by post-treatment with potassium thiocyanate, *J. Solid State Chem.* 2019, vol 269, 367−374, 2019

59 J. Liu, S.K. Pathak, N. Sakai, R. Sheng, S. Bai, Z. Wang, H.J. Snaith, Identification and Mitigation of a Critical Interfacial Instability in Perovskite Solar Cells Employing Copper Thiocyanate Hole-Transporter, *Adv. Mater. Interfaces*, vol 3, 1600571, 2016

60 Y. Chen, Z. Yang, X. Jia, Y. Wu, N. Yuan, J. Ding, W.H. Zhang, S. Liu, Thermally stable methylammonium-free inverted perovskite solar cells with Zn^{2+} doped $CuGaO_2$ as efficient mesoporous hole-transporting layer, *Nano Energy* ,vol 61, 148−157, 2019

61 P. Qin, T. Wu, Z. Wang, L. Xiao, L. Ma, F. Ye, L. Xiong, X. Chen, H. Li, X. Yu, G. Fang, Grain Boundary and Interface Passivation with Core–Shell Au@CdS

Nanospheres for High-Efficiency Perovskite Solar Cells, *Adv. Func. Mater.,* vol 30, 1908408, 2020

62 J. Peng, J. I. Khan, W. Liu, E. Ugur, T. Duong, Y. Wu, H. Shen, K. Wang, H. Dang, E. Aydin, X. Yang, Y. Wan, K. J. Weber, K. R. Catchpole, F. Laquai, S. D. Wolf, T. P. White, Efficient Indium-Doped TiOx Electron Transport Layers for High-Performance Perovskite Solar Cells and Perovskite-Silicon Tandems, *Adv. Energy Mater.,* vol 8, 1801208, 2018

63 F. Zhang, J. Song, R. Hu, Y. Xiang, J. He, Y. Hao, J. Lian, B. Zhang, P. Zeng, J. Qu, Interfacial Passivation of the p-Doped Hole-Transporting Layer Using General Insulating Polymers for High-Performance Inverted Perovskite Solar Cells, *Small,* vol 14, 1704007, 2018

64 M. Kim, S. G. Motti, R. Sorrentino, A. Petrozza, Enhanced solar cell stability by hygroscopic polymer passivation of metal halide perovskite thin film, *Energy Environ. Sci.,* vol 11, 2609, 2018

65 E. H. Jung, N. J. Jeon, E. Y. Park, C. S. Moon, T. J. Shin, T.Y. Yang, J. H. Noh, J. Seo, Efficient, stable and scalable perovskite solar cells using poly(3-hexylthiophene), *Nature* , vol 567, 511, 2019

66 C. Chen, X. Zhuang, W. Bi, Y. Wu, Y. Gao, G. Pan, D. Liu, Q. Dai, H. Song, Chemical inhibition of reversible decomposition for efficient and super-stable perovskite solar cells, *Nano Energy*, vol 68, 104315, 2020

67 Z. Wang, X. Zhu, S. Zuo, M. Chen, C. Zhang, C. Wang, X. Ren, Z. Yang, Z. Liu, X. Xu, Q. Chang, S. Yang, F. Meng, Z. Liu, N. Yuan, J. Ding, S. Liu, D. Yang, 27%-Efficiency Four-Terminal Perovskite/Silicon Tandem Solar Cells by Sandwiched Gold Nanomesh, *Adv. Funct. Mater.,* vol 30, 1908298, 2020

68 H. Zhou, Q. Chen, G. Li, S. Luo, T. Song, H. S. Duan, Z. Hong, J. You, Y. Liu, Y. Yang, Interface engineering of highly efficient perovskite solar cells, *Science,* vol 345, 542, 2014

69 C. Motta, F. El-Mellouhi, S. Sanvito, Charge carrier mobility in hybrid halide perovskites, *Sci. Rep.*, vol 5, 12746, 2015

70 T. M. Brenner, D. A. Egger, L. Kronik, G. Hodes, D. Cahen, Hybrid organic—inorganic perovskites: low-cost semiconductors with intriguing charge-transport properties, *Nat. Rev. Mater,* vol 1, 15007, 2016

71 W. S. Yang, J. H. Noh, N. J. Jeon, Y. C. Kim, S. Ryu, J. Seo, S. Seok, High-performance photovoltaic perovskite layers fabricated through intramolecular exchange, *Science,* vol 348, 1234, 2015

72 D. Bi, W. Tress, M.I. Dar, P. Gao, J. Luo, C. Renevier, K. Schenk, A. Abate, F. Giordano, J.P.C. Baena, J. D. Decoppet, S. M. Zakeeruddin, M.K. Nazeeruddin, M. Grätzel, A. Hagfeldt, Efficient luminescent solar cells based on tailored mixed-cation perovskites, *Sci. Adv.,*vol 2, 1501170, 2016

73 A. A. Asif, R. Singh, and G. F. Alapatt, Technical and economic assessment of perovskite solar cells for large scale manufacturing, *J. Renewable and Sustainable Energy*, vol 7, 043120, 2015

74 M. Z. Kabir, A Physics-Based Analytical Model for Current–Voltage Characteristics of Perovskite Solar Cells Incorporating Bulk Recombination, *Energies,* vol 14, 3868, 2021.

75 R. Wang, J. Xue, K.-L. Wang, Z.-K. Wang,Y. Luo, D. Fenning, G. Xu, S. Nuryyeva, T. Huang, Y. Zhao, J. L. Yang, J. Zhu, M. Wang, S. Tan, I. Yavuz, K. N. Houk, Y. Yang, Constructive molecular configurations for surface-defect passivation of perovskite photovoltaics, *Science,* vol 366, 6472, 2019

76 M. S. Anjan, M. Z. Kabir, Modeling of current–voltage characteristics of CdS/CdTe solar cells, *Phys. Status Solidi A,* vol 208, 1813, 2011

77 S. M. Arnab, M. Z. Kabir, An analytical model for analyzing the current-voltage characteristics of bulk heterojunction organic solar cells, *J. Appl. Phys.,* vol 115, 034504, 2014

78 L.F. Hernández-García, V. Cabrera-Arenas, L. M. Reséndiz-Mendoza, On the convergence of the algorithm for simulating organic solar cells, Comput. Phys. Commun., vol 196, 372, 2015.

79 W. Shockley, Currents to Conductors Induced by a Moving Point Charge, *J. Appl. Phys.* , vol 9, 635,1938.

80 Z. He, Review of the Shockley–Ramo theorem and its application in semiconductor gamma-ray detectors, *Nucl. Instr. Meth. Phys. Res. A,* vol 463, 250, 2001

81 M. A. Mannan, M. S. Anjan, M. Z. Kabir, Modeling of current–voltage characteristics of thin film solar cells, *Solid State Electronics,* vol 63, 49, 2011

82 M. M. Saleheen, S. M. Arnab, M. Z. Kabir, Analytical Model for Voltage-Dependent Photo and Dark Currents in Bulk Heterojunction Organic Solar Cells, *Energies*, vol 9, 412, 2016

83 National Renewable Energy Laboratory. Available online: http://rredc.nrel.gov/solar/spectra/am1.5/ (accessed on 6 October 2023)

84 J. M. Ball, A. Petrozza, Defects in perovskite-halides and their effects in solar cells, *Nat Energy* Vol 1, 16149, 2016

85 P. Wang, R. Li, B. Chen, F. Hou, J. Zhang, Y. Zhao, X. Zhang, Gradient Energy Alignment Engineering for Planar Perovskite Solar Cells with Efficiency Over 23%, *Advanced Material,* vol 32, 1905766, 2020

86 C.C. Zhang, S. Yuan, Y.-H. Lou, Q.-W. Liu, M. Li, H. Okada, Z.-K. Wang, Perovskite Films with Reduced Interfacial Strains via a Molecular-Level Flexible Interlayer for Photovoltaic Application, *Advanced Material,* vol 32, 2001479, 2020